

Core Radio and Optical Emission in the Nuclei of Nearby FR I Radio Galaxies¹

Gijs A. Verdoes Kleijn,² Stefi A. Baum,³ P. Tim de Zeeuw,²
Christopher P. O’Dea³

ABSTRACT

In this paper we analyze the relation between radio, optical continuum and $H\alpha$ + $[NII]$ emission from the cores of a sample of 21 nearby Fanaroff & Riley type I galaxies as observed with the VLBA and HST. The emission arises inside the inner tens of parsec of the galaxies. Core radio emission is observed in 19/20 galaxies, optical core continuum emission is detected in 12/21 galaxies and $H\alpha$ + $[NII]$ core emission is detected in 20/21 galaxies. We confirm the recently detected linear correlation between radio and optical core emission in FR I galaxies and show that both core emissions also correlate with central $H\alpha$ + $[NII]$ emission. The tight correlations between radio, optical and $H\alpha$ + $[NII]$ core emission constrain the bulk Lorentz factor to $\gamma \sim 2 - 5$ and $\gamma \lesssim 2$ for a continuous jet and a jet consisting of discrete blobs, respectively, assuming jet viewing angles in the range $[30^\circ, 90^\circ]$. Radio and optical core emissions are likely to be synchrotron radiation from the inner jet, possibly with a significant contribution from emission by an accretion disk and/or flow. Elliptical galaxies with LINER nuclei without large-scale radio jets seem to follow the core emission correlations found in FR I galaxies. This suggests that the central engines could be very similar for the two classes of AGNs.

Subject headings: galaxies: active — galaxies: elliptical and lenticular, cD — galaxies: nuclei — galaxies: structure — ISM: dust, extinction.

1. Introduction

Many galaxies in the nearby universe ($z < 0.1$) contain an active galactic nucleus (AGN) which features a central low-ionization narrow emission-line region (LINER). These AGNs typically have a bolometric luminosity $L_{\text{bol}} \lesssim 10^{43}$ erg s⁻¹ which is orders of magnitude smaller than those of classical AGN at higher redshifts, such as Seyferts, Quasars and Broad-line Radio Galaxies. The energy for the activity is thought to be provided by accretion of matter onto a supermassive black hole residing at the galaxy center in all AGN classes. Radio galaxies constitute a subset of the

¹Based on observations with the NASA/ESA Hubble Space Telescope obtained at the Space Telescope Science Institute, which is operated by the Association of Universities for Research in Astronomy, Incorporated, under NASA contract NAS5-26555.

²Sterrewacht Leiden, Postbus 9513, 2300 RA Leiden, The Netherlands.

³Space Telescope Science Institute, 3700 San Martin Drive, Baltimore, MD 21218.

active galaxy family. These galaxies have radio cores at their centers from which jets emerge. Radio galaxies are divided in two classes based on differences in large-scale radio morphology: low-power Fanaroff & Riley (1974) type I (FR I) radio galaxies and high-power radio FR II galaxies (cf. Bridle & Perley 1984). Many nearby FR I nuclei show optical LINER emission (e.g., Baum, Zirbel & O’Dea 1995). The goal of this paper is to study the active cores of nearby FR I galaxies and the relation to their nearby LINER-type counterparts without radio jets.

The hosts of FR I galaxies are almost without exception bright early-type galaxies (see Ledlow et al. 2001 for counter example). Quiescent and FR I radio galaxies in nearby Abell clusters show no statistical differences in their global properties (Ledlow & Owen 1995). The two classes do not differ in surface-brightness profiles, the surface-brightness and size relations, the distribution over ellipticities, and the occurrence and strength of non-elliptical isophotes. Zirbel (1993, 1996) found that FR I galaxies are larger than radio-quiet galaxies at given isophotal magnitude, but this result was not confirmed by Ledlow & Owen (1995). Ledlow & Owen (1995) did not find differences between the radio-loud and quiescent cluster galaxies in the local density of nearby companions, and in the frequency of morphological peculiarities or tidal interactions. Studies of samples of FR I galaxies either in the field or in small groups found indications of tidal interactions in a majority of them (Gonzalez-Serrano & Carballo 1993; Colina & de Juan 1995). It is unknown if this rate is different for quiescent galaxies in similar environments. In summary, it is unlikely that host environment and host global properties are decisive for the capability of an early-type galaxy to become a FR I galaxy, but tidal interactions might trigger the nuclear activity, at least in some cases.

With the advent of HST it has become possible to look for host galaxy differences closer to the AGN itself. In a previous paper (Verdoes Kleijn et al. 1999) we presented WFPC2 broad- and narrow-band images of a well-defined complete sample of 21 nearby FR I early-type UGC galaxies, the ‘UGC FR I sample’. Similar WFPC2 surveys of radio galaxies have been carried out also for the 3CR sample (Martel et al. 1999; de Koff et al. 2000) and the B2 sample (Capetti et al. 2000). The UGC FR I sample WFPC2 data suggest that the stellar content (i.e., color and shape) is very similar to that of quiescent early-type galaxies including the central few kiloparsec. However, a rigorous comparison with a quiescent galaxy sample to discern subtle differences has not yet been performed. Potential AGN fuel is clearly present in the inner hundreds of parsecs. Central $H\alpha + [\text{NII}]$ emission is detected in all sample galaxies and dust is detected in 19/21 galaxies. Other samples of FR I galaxies show emission-line detection rates of $\gtrsim 80\%$ (e.g., Baum & Heckman 1989; Morganti et al. 1992). The detection rate of small-scale dust in quiescent early-type galaxies is typically only $\sim 40\%$ (van Dokkum & Franx 1995; Tran et al. 2001), while emission-line gas is detected in typically $\sim 60\%$ of the quiescent early-type galaxy population (Philips et al. 1986; Goudfrooij et al. 1993). Thus, the detection rate of potential fuel for an AGN is lower but significant in quiescent galaxies and hence its presence seems not to be the only factor determining the on-set of activity.

A VLBA study of the radio properties of the cores and the inner jets in the UGC FR I nuclei has been presented by Xu et al. (2000). In this paper we analyze the correlation between this AGN radio emission and optical continuum and $H\alpha + [\text{NII}]$ core emission as observed with HST/WFPC2. We compare the UGC FR I core properties to those of 3CR FR I cores which have been studied

in the radio, optical and X-rays (e.g., Chiaberge, Capetti & Celotti 1999; Hardcastle & Worrall 2000). For the 3CR sample, the correlations between the core emissions have led to favor the inner jet as their origin. We determine the validity for different AGN components to produce the core emissions in the UGC FR I galaxies. We also compare the FR I core properties to those of nearby LINER-type AGNs without large-scale radio jets.

The outline of this paper is as follows. Section 2 describes the sample and data from the literature used in this analysis. It also describes in detail the optical core flux measurements. Section 3 quantifies the correlations between the core fluxes and shows they are not significantly affected by the ubiquitous central dust distributions. Section 4 describes the arguments against the existence of compact stellar clusters producing the optical core emission. We present evidence that the radio and optical cores are synchrotron emission from the inner jet and discuss constraints on its Doppler boosting. The contribution to the core emission by an accretion disk and/or flow is also considered. Section 5 discusses the possible excitation mechanisms for the central gas. Section 6 surveys the similarities between the FR I and other LINER cores. Section 7 summarizes the main results and final conclusions. Appendix A presents the WFPC2 imaging analysis for UGC 7115 and UGC 12064 (3C449). Appendix B discusses details of the beaming models used in Section 4.3.

Throughout the paper we use a Hubble constant $H_0 = 75 \text{ kms}^{-1}\text{Mpc}^{-1}$.

2. Sample and Data

The sample of 21 nearby FR I galaxies, which is limited in total radio flux, was constructed by positional cross-correlation of the Greenbank 1400 MHz sky maps and the UGC catalogue (Condon & Broderick 1988; Nilson 1973). The UGC FR I sample and its selection are described in more detail in Verdoes Kleijn et al. (1999, paper I).

2.1. Host Galaxy Imaging

We use the results from the HST/WFPC2 broadband imaging analysis for 19 of the 21 sample galaxies presented in paper I. In Appendix A we present the same analysis for the two remaining galaxies, UGC 7115 and UGC 12064 (3C 449). Their data reduction and isophotal analysis was carried out as described in detail in paper I.

2.2. Radio Observations

We use core and total flux densities from a VLA A imaging survey at 1490 MHz (FWHM $1.5'' - 3.75''$) (Wrobel, Machalski & Condon 2001) for the complete sample and from a VLBA imaging survey at 1670 MHz (FWHM $\sim 0.01''$) for 18 UGC FR I sample galaxies as presented by Xu et al. (2000). The VLA A core flux density of 3C 449 is taken from Feretti et al. (1999). UGC 7115 and 3C 449 lack VLBA observations because they were added to the sample only after the

VLBA observations were completed. NGC 3801 was not observed with the VLBA because no core was detected in the earlier VLA observation. Core radio fluxes at 5 GHz (FWHM $\sim 1.4''$ except NGC 4261: FWHM $\sim 15''$) for 11 sample galaxies are taken from Zirbel & Baum (1995). Total radio luminosities from the Greenbank 300 ft telescope at 1400 MHz (FWHM $12'$) for the complete sample are taken from Condon & Broderick (1988). Condon & Broderick corrected for confusion of the 1400 MHz total flux by nearby sources using VLA C observations (FWHM $18''$) for 12 of the UGC FR I galaxies. We verified that there was no confusion for the remaining nine UGC FR I galaxies using the NVSS catalog (FWHM $\sim 45''$; Condon et al. 1998).

2.3. Optical Core Emission

The nuclei of many sample galaxies reveal compact optical core emission in the WFPC2 *V*- and *I*-band images. To investigate the nature of these nuclear optical sources (NOS) we determine the unresolved flux at HST resolution after subtraction of the underlying galaxy light. For most galaxies we use the WFPC2 images presented in paper I. For NGC 4486 we use WFPC2 archival short-exposure observations (F555W and F814W 30s exposures, HST program 5477), since the observations in paper I have nearly saturated centers. For UGC 7115 and 3C 449 we use the images presented in Appendix A. The WFPC2 point spread function (PSF) has a FWHM $\sim 0.07''$ at *V* and *I* and 85% of the flux counts, which we want to isolate from the underlying galaxy light, are contained inside $r = 0.23''$. We approximate the underlying galaxy flux density inside $r = 0.23''$ by a constant. Its value is estimated by measuring the counts in an annulus with an inner radius of $0.23''$ (i.e., 5 PC pixels) and a width of $0.0455''$. After subtracting the underlying galaxy counts from the counts inside $0.23''$, we measure the resulting flux profile inside this radius. If this profile is consistent with being unresolved (i.e., FWHM in the range $0.05'' - 0.08''$) we decide there is a point source present in addition to the stellar light. The NOS counts were converted to fluxes using the ‘photflam’ values given in the HST Handbook (ed. Voit 1998). We correct the fluxes for Galactic fore-ground extinction and the 15% PSF flux which falls outside the $0.23''$ aperture.

Determination of the underlying stellar light can be difficult because dust is often present and the stellar light profile is sometimes bright and steep (cf. Figure 1). In fact, our procedure tends to overestimate the NOS flux, since galaxies typically have surface brightness profiles which are not constant but increasing towards the center. The irregular variations in the ubiquitous central dust obscuration inhibit accurate estimates of the individual central surface brightness slopes. Simulations indicate that our procedure would overestimate the NOS by typically 50% and at most a factor 2 for the galaxies with a NOS detected in the UGC FR I sample if central dust were not present. To estimate how the NOS flux estimate depends on aperture size, we determined the NOS using varying apertures in the range $0.13'' - 0.32''$. This typically results in NOS fluxes which differ by $\sim 30\%$. In addition to stellar galaxy light there is sometimes, depending on redshift, a contribution to the NOS flux from the [OIII] $\lambda\lambda 4959, 5007$ and $H\alpha + [NII]$ emission lines for the F547W and F555W and F702W filters. Using the central $H\alpha + [NII]$ fluxes from paper I and assuming $[OIII]/H\alpha + [NII] = 0.12$, typical for the LINER-type spectrum in FR I galaxies, we estimate that the contribution to the NOS flux in these filters is typically $\sim 15\%$ and at most 25%.

Given the aforementioned uncertainties and the difference in the spatial resolution of the broad- and narrow-band images, we did not attempt to correct the NOS for this emission-line contribution. The central dust might obscure the NOS and stellar background fluxes in several targets. We lack information on the nature of the dust obscuration to make a robust correction for internal dust obscuration. As an indication: if the observed opacity is caused by dust in front of the stellar flux and the NOS, then the observed $V - I$ WFPC2 colors typically imply correction factors ~ 1.5 for the V -band NOS fluxes. Given all uncertainties, we expect that the detected NOS fluxes are accurate to within a factor ~ 2 .

NOS were detected in 12 of the 21 galaxies. We estimate the expected NOS for the non-detections from the correlation between NOS and radio core and central $H\alpha + [\text{NII}]$ emission (see Section 3). We added the expected NOS counts artificially to the galaxy image as a scaled PSF to determine the possible reason for the non-detection. Adding the expected NOS indicates that it would be easily detected in NGC 741 (which has a shallow stellar surface brightness profile) and marginally detected in NGC 541, NGC 4335, NGC 5141, NGC 5490 and NGC 7626. NGC 541, NGC 4335, NGC 5490 and NGC 7626 have a bright and steep underlying stellar surface brightness profile which makes detection of a NOS difficult (cf., Figure 1). Thus these non-detections could be due to observational bias except for NGC 741. In fact, all NOS, except for UGC 7115, are detected in hosts with relatively shallow inner stellar surface brightness cusps. In the remaining three galaxies, NGC 3801, NGC 5127 and NGC 7052, the expected NOS could be hidden by foreground dust for plausible dust-extinction values. In NGC 7052, there is actually a hint of a very weak blue point source hidden behind the dust disk. For the galaxies with no obvious obscuration by foreground dust, the upper limit to the NOS flux was set to the flux measured within an aperture of $0.13''$ radius (i.e., 80% of the flux for an unresolved source) corrected for underlying stellar light. As a final check of the robustness of the NOS detection procedures, we verified that both NOS detections and upper limits do not correlate with the slope of the central stellar background flux profile.

Table 1 lists the NOS flux detections and upper limits. The V and I -band NOS fluxes generally differ by less than 50%. Our measurements agree typically within a factor < 2 with determinations by Chiaberge, Capetti & Celotti (1999) for seven overlapping targets. There is about a factor two disagreement between the F791W fluxes for UGC 7360 and the F702W fluxes for 3C 449. The former has a very weak NOS which makes the measurement difficult. Chiaberge et al. corrected the latter measurement for $H\alpha + [\text{NII}]$ which we estimated above to be about 15% of the NOS flux. This might explain part of the difference for this measurement.

In conclusion, a NOS is detected in $57\% \pm 16\%$ (21/21) of the FR I nuclei, dust might hide a NOS in another $14\% \pm 8\%$ (3/21), while upper limits to the NOS emission can be determined for $29\% \pm 12\%$ (6/21).

2.4. Central $H\alpha + [\text{NII}]$ Emission

The WFPC2 narrow-band imaging presented in paper I shows that the $H\alpha + [\text{NII}]$ emission is always dominated by a highly peaked nuclear component. Additional extended emission is detected

in several galaxies. Thus, in close analogy with the unresolved nuclear optical continuum analysis, we determined the nuclear unresolved $H\alpha+[NII]$ emission using the same procedure. We detected central $H\alpha+[NII]$ flux cores with $FWHM \lesssim 0.08''$ for the five targets with emission images on the PC detector and cores with a $FWHM \sim \lesssim 0.13''$ for 14 of the 15 targets on the WF2 detector. These $FWHM$ indicate that this emission component is consistent with being unresolved (the larger PSF $FWHM$ for the WF chip is caused by the larger WF pixel size ($0.0996''$) compared to the PC pixel size ($0.0455''$)). The $H\alpha+[NII]$ flux cores were unresolved at HST resolution in all UGC FR I galaxies except NGC 3801. For NGC 3801 we set the $H\alpha+[NII]$ flux in the central 9 pixels (75% of the PSF flux) as an upper limit. No WFPC2 $H\alpha+[NII]$ image is available for UGC 7115. In this case we estimated the core $H\alpha+[NII]$ flux from HST/STIS measurements, which will be published in a forthcoming paper. The core $H\alpha+[NII]$ fluxes are listed in Table 1. From estimates of the error in the stellar continuum subtraction and in the core flux measurement procedure we conclude that the core $H\alpha+[NII]$ fluxes are accurate to within 50%.

3. Correlations between Core Emissions

We now quantify the relation between nuclear radio, optical and $H\alpha+[NII]$ line emission. By definition the optical continuum and $H\alpha+[NII]$ core emission are unresolved at HST resolution ($FWHM \lesssim 0.1''$) which corresponds to a region on the order of a few tens of parsec or smaller. The VLBA cores are unresolved at a resolution of $FWHM \sim 0.01''$ and originates from a region smaller than a few pc in size.

3.1. Radio - $H\alpha+[NII]$ Core Correlation

The top two panels of Figure 2 we plot the central $H\alpha+[NII]$ emission as a function of VLBA core peak emission both as flux and luminosity for 18 sample galaxies. The two quantities are well correlated: both flux and luminosity correlations have a significance level $\geq 99.99\%$ using Kendall's tau test (see Tables 2 and 3). This gives us confidence that the correlation is not due to selection effects or a common dependence on distance. 3C274 (M87) is a slight outlier on the luminosity-luminosity correlation plot. This could be due to the fact that part of the $[NII]6584$ emission is redshifted out of the narrow-band filter (Ford et al. 1994). The alternative of Doppler boosting of the radio emission is discussed in Section 4.4. Two of the three missing objects, UGC 7115 and 3C 449, lack VLBA observations for reasons unrelated to their properties (see Section 2.2). No radio core was detected in NGC 3801. NGC 3801 has no detected core $H\alpha+[NII]$ emission. Thus we do not expect the missing objects to alter the correlations significantly. The luminosity-luminosity correlation extends over approximately two orders of magnitude in radio and $H\alpha+[NII]$ luminosity. A linear regression fit to the logarithmic values of the luminosities shows that the $H\alpha+[NII]$ luminosity is roughly proportional to the the radio core luminosity to the power 0.6 (Table 3).

How does this correlation compare with previous studies of FR I nuclei? Baum, Zirbel & O'Dea

(1995; see also Zirbel & Baum 1995, ZB95) performed an extensive study of a large sample of ~ 70 FR I galaxies, with radio and emission-line measurements gathered from the literature. Their FR I sample extends ~ 1 magnitude brighter in host magnitude and total and core radio luminosities. ZB95 found only a weak luminosity-luminosity correlation between integrated $H\alpha+[NII]$ emission and the radio core at 5 GHz (FWHM $\sim 1.4''$) for FR I galaxies. They found a much stronger correlation between integrated $H\alpha+[NII]$ emission and host magnitude. They also found a correlation with total radio luminosity, which turns out to be a weak (2σ) correlation after taking into account the correlation with host magnitude. ZB95 concluded that the $H\alpha+[NII]$ emission gas in FR I galaxies was most likely predominantly excited by radiation from old stars. Table 3 lists the parameters of the linear regression fits to the correlation between $H\alpha+[NII]$ emission and host optical magnitude and total radio power for the UGC FR I sample. The fits agree with those obtained by ZB95 after correction for the difference in the assumed value of the Hubble constant and difference in radio frequency. However, for the UGC FR I sample the resulting correlations are much weaker than the correlation between $H\alpha+[NII]$ and radio core. We compare the $H\alpha+[NII]$ luminosities for seven overlapping sources with $H\alpha+[NII]$ flux measurements in the UGC FR I and ZB95 sample. For four sources ZB95 report larger $H\alpha+[NII]$ luminosities. For the other three sources ZB95 actually use smaller $H\alpha+[NII]$ luminosities. However, from examination of the observational details there is clear indication for considerable uncertainty in each of these three measurements. Thus, the difference in correlation strength seems caused by the fact that we consider the core $H\alpha+[NII]$ fluxes, while ZB95 considered total fluxes, which might be dominated by an extended component. The correlation between the central $H\alpha+[NII]$ emission and radio core emission is also present if we restrict the sample to the 11 overlapping targets and use the 5GHz core emission values from ZB95 (see Tables 2 and 3). Similarly, there is a good correlation between the central $H\alpha+[NII]$ emission and the VLA core emission (FWHM $\sim 1.5'' - 3.75''$). It is significant at $> 99.9\%$ level and has a similar slope as the correlation with VLBA core emission (Tables 2 and 3). Thus the difference in spatial resolution of the VLBA, VLA and 5 GHz measurements does not seem relevant. The correlation with extended VLBA radio emission is significant at the $> 99\%$ level and has a similar slope. No strong correlation is found between the extended VLA emission and the $H\alpha+[NII]$ emission.

Thus not surprisingly, the AGN, which produces the radio core emission (see also discussion in Section 4.2), very likely excites the gas in the central few hundreds of parsec in the FR I nuclei. More interestingly, the excitation energy correlates tightly with the central radio power. The correlation between total $H\alpha+[NII]$ luminosity and host galaxy magnitude, as found by ZB95, probably indicates that the gas on kpc scales is excited by some other process(es) (e.g., radiation from old stars).

3.2. Radio - Optical Core Correlation

The middle two panels in Figure 2 plot the nuclear optical source emission in the I -band as a function of VLBA core peak emission both in flux and luminosity for 16 of the 21 sample galaxies. In six galaxies the NOS measurement is an upper limit. The two quantities are well correlated: both flux and luminosity correlations have a significance level larger than 99.9% using Kendall's

tau test, which takes the upper limits into account (see Tables 2 and 3). This gives us confidence that the correlation is not due to selection effects or a common dependence on distance. Figure 2 shows the correlation with the *I*-band NOS, because the *V*-band NOS can be more affected by dust obscuration. Both NOS emissions correlate well with the VLBA radio core (see Tables 2 and 3). Two of the five missing galaxies, UGC 7115 and 3C 449 both host a NOS (see Table 2) but lack VLBA observations for reasons unrelated to their properties (see Section 2.2). No NOS is detected in NGC 3801, NGC 5127 and NGC 7052, which could be due to large foreground dust obscuration (cf. Section 2.3). Thus all missing objects might host a NOS in principle. There is no a priori reason to believe that the missing targets will alter the correlation significantly. For five of the six upper limits, the NOS flux, as expected from the radio - optical core correlation, would be difficult to detect (cf. Section 2.3). The slope of the correlation between the logarithm of the VLBA core and the *I*-band optical core luminosities is 1.18 ± 0.25 (see Table 3). The slope for the *V*-band optical core is less constrained but slightly steeper: 1.47 ± 0.35 . Thus the majority of the 21 FR I nuclei do show NOS emission, which is roughly proportional to the radio core emission.

Chiaberge, Capetti & Celotti (1999) used HST/WFPC2 observations to determine optical core emission in all 33 FR I galaxies in the 3CR catalogue. They detected a NOS in $69\% \pm 15\%$ of the galaxies, dust could hide a NOS in $13\% \pm 6\%$, and no NOS was detected in $19\% \pm 8\%$. Thus, the detection rates for the 3CR FR I sample and UGC FR I sample are similar. Their NOS measurements agree well with our results for the seven overlapping 3CR galaxies (see Section 2.3). Chiaberge, Capetti & Celotti also found a linear correlation between radio and optical core flux. Figure 3 show the *I*-band NOS versus radio core flux for the 16 UGC galaxies and the 20 3CR galaxies which are not part of the UGC FR I sample. The radio core flux at 5 GHz is plotted for the galaxies taken from Chiaberge, Capetti & Celotti, as listed in their paper. For the UGC FR I sample, the VLA radio core flux at 1.49 GHz is actually plotted. The 5 GHz and 1.49 GHz observations have similar beamwidths. The measurements can therefore be compared directly under the assumption of flat spectral slopes. This seems to be a reasonable assumption because the fluxes in the UGC FR I galaxies with both 5GHz and 1.49 GHz observations typically differ by a factor < 2 . The combined sample of 37 FR I galaxies suggests a single relation between radio and optical core emission. The only outlier is 3C 386. As discussed by Chiaberge, Capetti & Celotti (1999), 3C 386 displays broad $H\alpha$ emission lines which is highly unusual for a FR I galaxy. We performed a linear regression fit using Kaplan-Meier residuals on the combined sample (Isobe, Feigelson & Nelson 1986). The outlier 3C386 is excluded from the fit. Both 3C 28 and 3C 314.1 are excluded from the fit as well because they have upper limits to both their radio and optical flux, which cannot be dealt with by the fitting routine. The linear fit to the logarithms of optical core flux as a function of radio core flux is significant at the $> 99.99\%$ level and has a slope of 1.0 ± 0.1 .

Hence, both the 3CR and UGC sample of FR I galaxies indicate a linear relation between radio and optical core emission. The proportionality makes a common origin for the radio and optical core flux plausible.

3.3. Optical - H α + [NII] Core Correlation

We should expect a correlation between nuclear optical core and central H α + [NII] emission, given the correlations between the radio core and H α + [NII] emission and between the radio and optical core. Any correlation, if present, might show considerable scatter due to the larger errors in optical core and H α + [NII] emission in comparison with the error in radio core flux.

The central H α + [NII] emission as a function of NOS emission is shown in the bottom panels of Figure 2 for 18 of the 21 galaxies. The three galaxies missing from the plot; the cores of NGC 3801, NGC 5127 and NGC 7052 are too obscured by dust to determine the NOS flux (cf. Section 2.3). It is not expected that the missing galaxies bias the relation between H α + [NII] and NOS emission. The optical core and central H α + [NII] emission are indeed correlated. The fluxes and luminosities are correlated at a significance larger than 99%, using Kendall’s tau test (see Tables 2 and 3). There are two outliers from the general relation: NGC 4261 and NGC 2329. In NGC 4261 the NOS is detected at the bottom of a dip in the central luminosity profile, which is due to dust obscuration. Thus, the intrinsic NOS flux might be severely dimmed. For NGC 2329 there is no clear indication that its NOS and/or H α + [NII] emission flux is biased. However, in paper I we noted a slight linear extension of the nuclear optical core. Possibly, an extra optical component (e.g., slightly extended optical jet) in NGC 2329 causes an overestimate of the NOS flux. The H α + [NII] and optical emission measurements have similar errors. Neither of the quantities can be considered an independent variable in a linear regression fit. We perform a linear least squares fit which takes into account the error in both optical core flux and H α + [NII] flux (Press et al. 1992). The method cannot take into account the data with upper limits, which however suggest a similar relation as the detections. The best fit to the logarithms of the H α + [NII] luminosity as a function of the NOS luminosity has a slope 0.55 ± 0.17 which is similar to the slope between H α + [NII] and radio core emission (Table 3).

3.4. Correlation between Regression Fit Residuals

There are three pairs of linear regression fits, each one with one of the three core luminosities as the independent variable and fitting the other two. We determined if a correlation exists between the residuals of each pair of fits. We see a trend instead of a scatter plot only if the central H α + [NII] luminosity is taken as the independent variable do (Figure 4). This is additional support for the view that the optical and radio core emission share a common origin.

3.5. Dust Obscuration

Paper I discusses the dichotomy in apparent dust morphology: (i) dust disks, which appear as smooth ellipses and (ii) dust lanes, which are irregular dust filaments. This extended central dust, detected in 19 of the 21 UGC FR I galaxies, might potentially obscure a significant fraction of the central optical line and continuum emission.

As a general check if dust affects the measurements of the optical continuum and $H\alpha+[NII]$ core emissions we checked for any correlation between the two core luminosities and IRAS far infrared luminosities which trace the extended hot dust (possibly with additional emission from stars) at 12 and 25 micron and cool dust at 60 and 100 micron (e.g., Knapp, Bies & van Gorkom 1990). IRAS flux measurements are available for 17 UGC FR I galaxies (Knapp et al. 1989). About half of those are flux upperlimits. No correlation or trend is observed for the $H\alpha+[NII]$ and optical core luminosities and any of the IRAS luminosities (see Table 3).

Another possibility is that the obscuration depends on the orientation of the central dust. For example, the amount of obscuration along the line of sight increases going from face-on disks to edge-on disks and/or dust lanes. Could this induce the correlation between $H\alpha+[NII]$ and optical core luminosity? Figure 2 shows that a large but not too unreasonable range in V -band dust opacity of $A_V \sim 5$ tends to spread the observed luminosities roughly along the observed correlation, if the intrinsic luminosities were quite similar among the sample. However, there is no correlation between either $H\alpha+[NII]$ or optical core luminosity and dust-disk inclination (Table 3; an inclination for the disks was derived by assuming intrinsically round disks, cf. paper I). The average $H\alpha+[NII]$ luminosity is slightly lower (~ 0.5 dex) in dust-lane galaxies than in dust-disk galaxies. Dust lanes might intersect the line of sight towards the $H\alpha+[NII]$ emission, while relatively face-on dust disks might not, or there might be an intrinsic difference in $H\alpha+[NII]$ luminosities of dust-disk and dust-lane galaxies. There is also no indication of significant foreground dust obscuration from the $V - I$ color of the optical core emission as a function of dust-disk inclination. Only a statistically insignificant trend is present (Table 3), for which the slope is too shallow to explain the observed range in luminosities. Thus, foreground dust does not appear to systematically affect the $H\alpha+[NII]$ and optical core emission. This makes it very unlikely as well, that dust obscuration induces the correlations of $H\alpha+[NII]$ and optical core emission as a function of radio core emission, which extend over two decades or more in luminosity.

Could foreground dust obscuration cause the scatter in the correlations of optical core and $H\alpha+[NII]$ luminosity as a function of radio core luminosity? The observed scatter of about one decade in both correlations requires a reasonable optical depth variation of $A_V \sim 3$ between the least and most obscured cases in the UGC FR I sample (see arrow in Figure 2). However, there is no trend between the residuals of the linear regression fits as a function of dust-disk inclination (Table 3). There is also no systematic difference between dust-disk and dust-lane galaxies.

3.6. Summary Core Emission Correlations

The conclusion from Section 3 is that the radio, optical and $H\alpha+[NII]$ core emission are all mutually well correlated. The analysis indicates that the optical core emission is proportional to the radio core emission. The central $H\alpha+[NII]$ emission is consistent with being roughly proportional to the square root of both optical and radio core emission. It is highly unlikely that variations in foreground dust obscuration cause the correlations between $H\alpha+[NII]$, optical and radio core emission. These correlations rather reflect physical connections between the three emissions. Foreground dust is also unlikely to induce the scatter in the correlations. We will show in Section 4.3

that Doppler boosting is a more viable explanation for the scatter (which probably contains an additional contribution from intrinsic scatter, flux variability and measurement errors as well).

4. Origin of the Optical and Radio Core Emission

We can use the observed correlations between the core emissions to constrain the origin of these emissions. We will consider the possibility that the optical core emission is produced by a compact nuclear stellar cluster. This will turn out to be implausible and we then go on to consider the possibility that the optical and radio core emissions originate in the unresolved inner jet and/or accretion disk or flow.

4.1. Compact Young Stellar Clusters?

There are two main methods to discriminate between a stellar and non-stellar origin for the optical core emission. First, sufficiently strong nuclear stellar absorption lines will indicate a stellar origin for the optical core emission. Second, the nuclear gas emission-line ratios can be used to distinguish between excitation by an AGN or stars. A spectral analysis of the optical core emission has been performed for the two nearest members of the UGC FR I sample, M84 and M87, at sufficient spatial resolution to isolate it from the stellar galaxy background. Bower et al. (2000) conclude that the nuclear continuum source in M84 is an AGN from the analysis of an HST/STIS optical spectrum (covering $\sim 2900 \text{ \AA} - 6800 \text{ \AA}$), taking into account the nuclear dust obscuration. The observed emission-line ratios exclude excitation by young massive OB stars, while the weakness of the stellar absorption features exclude a cluster of A stars. Last but not least, the variability of the optical core (75% in the V -band over a five year period) argues against a stellar origin for the optical core in M84. Dressler & Richstone (1990) and Kormendy (1992) argued that the nucleus in M87 has a non-thermal origin from the weakness of stellar absorption lines in the B - and V -band. Carter & Jenkins (1992) and van der Marel (1994) reached the same conclusion using ground-based optical and near-IR spectra. Both studies did not confirm the earlier detection of strong stellar Ca II triplet lines by Jarvis & Melnick (1991). Tsvetanov et al. (1999) determined from wide-band ($\sim 1600 \text{ \AA} - 8000 \text{ \AA}$) HST/FOS peak-up optical images that also the core of M87 varies by a factor ~ 2 over 2.5 months, a factor ~ 0.25 over three weeks and a factor < 0.025 over one day, which again strongly argues against a stellar origin for the optical core emission. Both M84 and M87 have optical core luminosities representative of the UGC FR I sample. Thus for two typical members of the 21 UGC FR I galaxies it has been convincingly shown that the optical core emission source is not a stellar cluster but must be AGN related.

It is possible that (some of) the 19 remaining UGC FR I nuclei do host a nuclear stellar cluster. In fact, such compact nuclear stellar clusters, with sizes smaller than a few tens of parsec, have been found in other galaxies. Maoz et al. (1998) performed a UV spectroscopic study of the compact nuclei of a sample of seven nearby UV-bright galaxies with LINER type emission using HST (cf. Table 4). Their nuclear SED appear similar to the UGC FR I galaxies, which also show LINER

emission and compact UV emission (Ho, 1999b; Ford et al. 1994; Ferrarese et al. 1996; van der Marel & van den Bosch 1998; Zirbel & Baum 1998). All seven UV nuclei from the LINER sample are compact and four are consistent with being unresolved, which implies scales of a few parsec (Maoz et al. 1995; Barth et al. 1998). Maoz et al. (1998) detected UV stellar absorption-lines in NGC 404, NGC 4569, NGC 5055 and possibly NGC 6500 and concluded that the dominant UV continuum source is a cluster of young massive stars in these galaxies. An AGN is most likely the UV continuum source in NGC 3031 and NGC 4579, which show broad UV emission lines and in NGC 4594, which has narrow UV emission lines (cf. Nicholson et al. 1998). We will refer to the former four galaxies as stellar-type LINERS and to the latter three as AGN-type LINERS.

We reduced HST/WFPC2 archival optical images for the LINER sample to study the optical cores (see Table 4). We determined the unresolved NOS flux in six of the seven galaxies in the same manner as done for the UGC FR I galaxies (cf. Section 2.3). Unfortunately, the core of NGC 5055 was saturated. We find an unresolved optical core in all six LINER galaxies except NGC 6500. The same result was derived for the UV cores, using detailed PSF modeling. In NGC 4569 the optical core was unresolved in the V -band but slightly resolved in the I -band. As opposed to Maoz et al. (1995), Barth et al. (1998) also detect slightly resolved UV emission in NGC 4569, which however is strongly peaked towards the nucleus. Our NOS fluxes agree within a factor of ~ 2 with measurements by Ho (1999b) for three overlapping targets. The agreements in the spatial extent and flux measurement of the nuclear optical emission support the idea that our simple method for detecting and measuring unresolved emission is accurate for our purposes. Table 4 lists the optical core fluxes and central $H\alpha+[NII]$ and 1.4 GHz radio luminosities for the LINER sample gathered from the literature.

Figure 5 shows again the correlations between the central luminosities for the UGC FR I sample but now with the LINER sample data overplotted. The AGN-type LINERS and UGC FR I galaxies have similar NOS and $H\alpha+[NII]$ luminosities. The LINER $H\alpha+[NII]$ luminosities are measured in apertures of typically a few arcsecond radius and hence overestimate the core $H\alpha+[NII]$ luminosity. Taking this into consideration, the AGN-type LINERS seem roughly to extend the core emission relations of the UGC FR I sample. The stellar-type LINERS also have similar NOS luminosities. NGC 4569 has a comparable $H\alpha+[NII]$ luminosity as well, but NGC 404 has an order of magnitude lower $H\alpha+[NII]$ luminosity. Furthermore, the upper limits to the radio core luminosities of the stellar-type LINERS are significantly below those of UGC FR I galaxies except for one (NGC 6500). Thus, in general the AGN-type LINER nuclei resemble the UGC FR I nuclei in their core emission properties more closely than the stellar-type LINERS. It is especially the radio core luminosity that separates the stellar-type LINERS from the AGN-type LINERS and UGC FR I galaxies. The core radio emission in the UGC FR I nuclei is certainly non-thermal AGN emission (cf. Section 4.2). The resemblance with the AGN-type LINERS suggest an AGN source for the optical continuum and line emission in all UGC FR I nuclei is more likely than a stellar origin. It is unlikely that systematic differences in obscuration by central dust, which is commonly present in both stellar- and AGN-type LINER and UGC FR I galaxies, conspire to produce the overlap and separation of the nuclear luminosities. Indeed, the $V - I$ colors of the LINER cores (only available for NGC 4579 and NGC 4594) and the UGC FR I cores are similar.

We conclude that a stellar origin for the optical core emission is highly unlikely for two reasons.

First, previous spectral studies have directly excluded a nuclear stellar cluster as the source of the optical core emission for two typical members of the UGC FR I sample. Second, the UGC FR I nuclei resemble the nuclei of AGN-type LINERS more closely than stellar-type LINERS in their radio and optical core and central $H\alpha$ + $[NII]$ luminosities. In contrast, an AGN origin for the optical cores in all UGC FR I galaxies is strongly favored by the tight correlation with radio core emission, which is certainly produced by the AGN.

4.2. Jet Synchrotron Emission

We shift our attention to a scenario in which the radio and optical core emission originate in the inner jet. The radio core emission in radio galaxies is generally thought to be self-absorbed non-thermal synchrotron emission because it has a high degree of polarization, a high brightness temperature and typically a flat spectral slope at radio wavelengths (cf. Krolik 1999 for a general discussion). The tight linear relation between radio and optical core flux (see Section 3.2) then suggests that the optical core emission is also jet synchrotron emission. It is therefore useful to compare the cores to extended optical jets, in which both radio and optical emission are commonly thought to be synchrotron emission (e.g., Lara et al. 1999). The radio-to-optical spectral index α_{ro} (defined by $S_\nu \sim \nu^{-\alpha}$) of the UGC FR I cores varies between 0.44 and 0.86 using any combination of either V - or I -band NOS and either VLA or VLBA core fluxes. These values are consistent with those found for extended optical jets in the UGC FR I sample: 3C 66B, 3C 264 and M87 (Butcher, van Breugel & Miley, 1980; Biretta et al. 1991; Lara et al. 1999). The spectral index might be affected by core flux variability, because the optical and radio observations were made at different epochs. The optical cores in M84 and M87 are known to vary by a factor of a few (see Section 4.1). Not much is known about the flux variability of radio cores in FR I galaxies, but a factor of a few seems reasonable (Shukla & Stoner 1996). As an indication, a flux ratio variation of a factor of 10 results in α_{ro} variation of ~ 0.2 . Although the V - and I -band observations were made at the same epoch, the V -to- I spectral index, α_{VI} , is much less secure than α_{ro} , due to the large relative errors of the optical core fluxes and the shorter frequency range (the error in α_{VI} is approximately 6 times the error in the logarithm of the flux ratio). We determined α_{VI} taking into account the filter passbands (using `calphot` in the IRAF `synphot` package). Extended optical jets have been detected in three UGC FR I galaxies: 3C 66B, 3C 264 and 3C 274. The optical spectral index of the core emission is very similar to that of the extended jet emission in 3C 264 and M87. The optical jet in 3C 66B is too faint to make a reliable comparison. For the complete sample of UGC FR I cores, we determine $\alpha_{VI} \sim 1 - 2$ typically, which is again in the same range as found for extended optical jets (e.g., Crane et al. 1993 and references therein; Biretta et al. 1991; Martel et al. 1998). However, steeper spectral indices up to $\alpha_{VI} \sim 5$ are observed as well. In addition to the large measurement uncertainty, any foreground dust (either present in our Galaxy or the galaxy itself) will steepen the observed optical core spectral index. For example, if one uses the spectral flux density at 5500 Å and 8000 Å to compute the spectral index and assume foreground dust with Galactic reddening law then $\alpha_{obs} = \alpha_{int} + 0.2A_V / \log(\nu_V / \nu_I) \approx \alpha_{int} + 1.2A_V$. Hence extinction from foreground dust could account for the steeper optical spectral indices.

Thus two conclusions can be drawn. First, the tight linear correlation between optical and radio core flux strongly suggests that also the optical cores are synchrotron emission. Second, the similarities in radio and optical emission from extended jets are consistent with both core emissions originating in an unresolved inner jet.

4.3. Doppler Boosting of Core Emission

If indeed radio and optical core emission originate in the inner jet both continuum emissions could be significantly Doppler boosted. This is in contrast with the $\text{H}\alpha + [\text{NII}]$ core emission, which is very likely not Doppler boosted. We will assume in the following that the $\text{H}\alpha + [\text{NII}]$ flux is emitted isotropically and not affected by dust obscuration, based on the results in Section 3.5. We will further assume that the radio and optical core emission originates from a symmetric jet. The logarithmic factor \mathcal{B} by which the core flux is (de-)boosted is then (cf. Appendix B)

$$\begin{aligned} \mathcal{B} &= \log \frac{\delta^p(\theta) + \delta^p(\pi + \theta)}{2}, \\ \delta(\theta) &= [\gamma(1 - \beta \cos \theta)]^{-1}, \end{aligned} \tag{1}$$

where γ is the bulk Lorentz factor, β the jet velocity in units of the velocity of light, θ the jet viewing angle and p the jet structural parameter. The value of p for FR I jets is not known. We will consider two cases: (i) a continuous jet isotropically emitting in the source rest-frame (i.e., $p = 2 + \alpha$) and (ii) a jet consisting of discrete blobs isotropically emitting in the source rest-frame (i.e., $p = 3 + \alpha$) (see e.g., Urry & Padovani 1995). For simplicity we will assume a flat core radio spectrum in the source rest frame (i.e., $\alpha = 0$).

In Appendix B we determine the effect of Doppler boosting on the observed correlation of fluxes which are intrinsically related by a power law. The main effect is to introduce scatter in the observed relationship. The scatter increases with γ for a given p and given range in jet viewing angles. We will first infer γ assuming that the viewing angles, θ , are randomly spherically distributed in the range $[30^\circ, 90^\circ]$, which is plausible for the UGC FR I jets (see also Section 4.4). We then discuss the critical dependence of the results on the assumed range in viewing angles.

Thus we can infer a typical γ for the sample from the observed standard deviation of ~ 0.3 for the linear regression fit of the VLBA radio core flux as a function of $\text{H}\alpha + [\text{NII}]$ flux in log-log space. Figure 6a plots predicted standard deviations as a function of a constant bulk Lorentz factor γ for $p = 2$ and $p = 3$. For the continuous jet the observed standard deviation corresponds to a typical bulk Lorentz factor $\gamma \approx 2.7$ (for $\theta = [30^\circ, 90^\circ]$). For a jet consisting of discrete blobs the observed standard deviation corresponds to $\gamma \approx 1.5$. The linear regression fits to the VLA core or VLBA extended emission instead of the VLBA core emission also have standard deviations ~ 0.3 . Hence similar constraints on p and γ are derived for the radio emission at these scales. The scatter in the optical - $\text{H}\alpha + [\text{NII}]$ core correlation has a standard deviation ~ 0.5 . This larger value (compared to the radio core correlation) could be consistent with the same γ as inferred for the radio cores if it is caused by the larger relative measurement error of the optical core emission. Indeed, the observed standard deviations are probably only partially due to Doppler boosting, because intrinsic scatter, flux measurement errors and perhaps other effects contribute to the observed scatter. In fact the

mean error in the central $\text{H}\alpha + [\text{NII}]$ flux is $\log 1.5 \approx 0.2$. Thus any inferred γ is likely to be an upper limit (cf. Figure 6a).

Another constraint on γ can be derived from the observed range in residuals. The observed range in residuals is $\sim [-0.5, 1.0]$ (cf. Figure 4). Figure 6b shows the predicted range in residuals for different p and γ . For the continuous jet ($p = 2$) the observed range is reproduced for $\gamma \approx 5$, while for the jet consisting of discrete blobs ($p = 3$) the observed range is reproduced for $\gamma \approx 2$. Interestingly the predicted asymmetry around 0 in the spread of the residuals is present in the observations as well.

Thus, for $p = 2$ the observed range in residuals suggests a significant spread around the typical Lorentz bulk factor $\gamma = 2.7$ derived from the spread of the sample as whole with some jets reaching $\gamma = 5$ at least. For $p = 3$ both the total range and dispersion of the residuals is consistent with $\gamma \lesssim 2$.

There is further circumstantial evidence that the spread around the linear regressions is indeed caused by Doppler boosting. On the one hand, Xu et al. (2000) note that NGC 2892, NGC 4335, NGC 5127 and possibly NGC 7626 do not have extended structures associated with the VLBA radio cores and that their large scale jets are more symmetric than those in the other UGC FR I galaxies. As argued by Xu et al., a possible scenario is that these jets lie close to the plane of the sky and hence have VLBA jets deboosted below the detection threshold. At larger scales the jets are slowed down and hence have negligible Doppler boosting. On the other hand, there is evidence that extended optical jets are only detected when the jet angle is sufficiently close to the line of sight (Sparks et al. 1995; Sparks et al. 2000). Extended optical jet emission has been detected in three UGC FR I sample galaxies: 3C66B, 3C264 and M87. Figure 7 plots the residuals as a function of radio and optical core luminosity. For the radio residuals, all the galaxies without extended VLBA structures have negative residuals while all galaxies with extended optical jets have positive or close to positive residuals. There is also a trend for more luminous cores to have more positive residuals. This is expected if the increase in core luminosity is (at least partially) caused by Doppler boosting. The corresponding plot for the optical core emission is consistent with these results. It shows more scatter, which is expected as the errors in the optical core flux are larger than those of the radio core flux. Finally, the correlation between the residuals of the optical/radio core correlations with $\text{H}\alpha + [\text{NII}]$ emission suggest they are Doppler boosted as well (cf. Figure 4). The trends are mainly driven by the few points at the high and low end of the distributions and hence larger samples are required to confirm these results.

The bulk Lorentz factors inferred above depend on the assumptions of $\alpha = 0$ and the range in jet viewing angles $[\theta_0, \theta_1]$. Our model depends on α only through $p = p_0 + \alpha$, where $p_0 = 2, 3$. Thus varying α is identical to varying p , which is discussed above. The results depend critically on the assumed minimum jet angle θ_0 because Doppler boosting increases rapidly as a function of θ at small θ (Figure 6b). Figure 6 illustrates the effect of varying θ_0 between $[20^\circ, 40^\circ]$.

BL Lac galaxies are commonly thought to be a subset of FR I galaxies where the jet is pointed very close to the line of sight (e.g., Browne 1983; Urry & Padovani 1995). This FR I-BL Lac unification scheme typically requires larger bulk Lorentz factors, $\gamma > 5$, than inferred by our analysis. In general, BL Lac jet studies infer a larger γ than FR I jet studies (Urry & Padovani

1995). Two-layer jets have been invoked to reconcile this apparent discrepancy. A fast inner spine is surrounded by a slower outer layer with. In FR I galaxies the jet emission is dominated by the slow outer layer and in BL Lac galaxies by the fast spine. For example, Chiaberge et al. (2000) argue for a two-velocity jet, based on the core optical, radio and X-ray fluxes assuming that these fluxes are dominated by jet emission. They infer a fast inner spine with $\gamma \sim 15 - 20$ surrounded by a slower outer layer with $1 < \gamma \lesssim 2$. These results are derived using jet de-beaming models of BL Lac SEDs for $p = 3$. So this two-velocity component jet model infers the same $\gamma \lesssim 2$ as derived by us from the correlation between radio core flux and central $H\alpha + [NII]$ flux for our UGC FR I sample for $p = 3$ and $\theta = [30^\circ, 90^\circ]$. Additional evidence for the presence of two-velocity jets comes from detailed modeling of extended FR I jets (e.g., Owen, Hardee & Cornwell 1989; Komissarov 1990; Hardcastle et al. 1996; Laing et al. 1999). Giovannini et al. (2001) use the scatter in the correlation between VLBI core and total radio power for a sample of 13 FR I, 6 FR II and 8 compact radio objects to derive $\gamma \sim 3 - 10$ for the cores under the assumption of $p = 2$. The $\gamma \sim 2 - 5$ derived by our method is roughly consistent with this, especially since lower bulk Lorentz factors are typically expected in FR Is compared to FR IIs.

Thus our constraints on γ from the tight correlation between radio core and $H\alpha + [NII]$ emission agree with constraints on γ from other methods. To establish whether cores are mildly or non-relativistic (i.e., $\gamma \lesssim 2$) or highly relativistic (i.e., $\gamma > 2$) requires precise knowledge of the jet structure since the inferred value of γ of the core emission critically depends on the value of p within the typically assumed range $p = 2 - 3$ and the range in jet viewing angles and how much of the scatter is due to non-Doppler boosting effects.

4.4. Accretion flow emission

The absence of compelling evidence for bulk Doppler boosting with $\gamma > 2$ leaves open the possibility that a component, different from the inner jet, dominates the radio and optical core emission. For example, it could be synchrotron (and/or inverse Compton) emission from the accretion disk and flow or wind. The inferred bolometric AGN luminosities of LINER and UGC FR I sample galaxies are three to five orders of magnitude below the Eddington luminosities (Ho 1999b). They are therefore more easily explained by advection dominated accretion flows (ADAF) than standard, geometrically thin, optically thick accretion disks. In these models the radio emission is synchrotron emission and the optical emission is synchrotron and/or inverse Compton emission (e.g., Narayan, Mahadevan & Quataert 1998). Quataert, Di Matteo & Narayan (1999) obtain a reasonable fit to the central radio to X-ray spectral energy distribution (SED) of two AGN-type LINER galaxies NGC 3031 and NGC 4579, which have unresolved nuclear cores with SEDs similar to the UGC FR I galaxies (cf. Section 4.1). The authors use a combination of a standard thin accretion disk with an ADAF model for the inner accretion disk. However, the best-fit model critically depends on the amount of dust obscuration for the optical and UV fluxes. For the core of M87, an ADAF model by Reynolds et al. (1996) underpredicts the optical flux by a factor of > 100 . More recently, Di Matteo et al. (2000) obtain a reasonable fit to the radio to X-ray SED of M87 using an ADAF model combined with an outflow. The models that fit the observed X-ray SED

underpredict the nuclear optical emission by a factor of ~ 5 . Di Matteo et al. note evidence for nuclear synchrotron jet emission from the radio and millimeter fluxes. Perhaps the X-ray emission also contains a beamed component. Yi & Boughn (1999) show that ADAF models predict within a factor of a few the radio core fluxes in NGC 4261, NGC 4374 and M87.

Thus, ADAF type models seem to provide a reasonable global fit to the nuclear SEDs of AGN-type LINERS which are similar to UGC FR I AGNs, but tend to underpredict the optical and radio core flux in UGC FR I galaxies. For the well-studied galaxy M87, jet viewing angles in the range $\sim 20^\circ - 40^\circ$ have been reported (Biretta, Zhou & Owen 1995; Biretta et al. 1999). Already for $\gamma = 2$, logarithmic Doppler boosting factors \mathcal{B} (cf. 4.3) vary by $\Delta\mathcal{B} = 0.91$ and $\Delta\mathcal{B} = -1.5$ between viewing angles $\theta = 30^\circ$ and $\theta = 90^\circ$ for $p = 2$ and $p = 3$, respectively. Thus the factors by which the optical and radio core emission is underpredicted in the ADAF model for M87 could be on the order of the variation in Doppler deboosting factors with jet viewing angle.

M87, the nearest galaxy in the sample, offers the possibility to directly localize the origin of the radio core emission at the highest attainable spatial resolution. Junor, Biretta & Livio (1999) obtained extreme high-resolution VLBI imaging (beam size 0.33mas x 0.12mas) at 43 GHz of the core of M87. The image shows that the jet does not obtain its final collimation (as observed at pc and kpc scale) until a few parsec from the core. Even at this high spatial resolution, there is still a dominant core component of size $\lesssim 0.5\text{mas}$. This corresponds to 0.04 pc or 130 Schwarzschild radii ($r_s = 2GM_{\text{BH}}/c^2$) for M87. The peak flux density is 228 mJy/beam, while the VLBA core flux density at 1.49 GHz is 1570 mJy/beam at a resolution of 10mas x 10mas. Hence a decrease by a factor of 2500 in beam area corresponds to only a decrease by a factor 7 in peak flux density. The VLBA core emission could therefore originate at the same scale as the VLBI core emission. The flux difference might then be due to radio core variability. Alternatively, the flux difference between 1.4 GHz and 43 GHz corresponds to a radio spectral index of 0.57. Thus, it is possible for at least M87 that the VLBA core flux (FWHM $\sim 0.01''$) is dominated by a nuclear component which resides at radii smaller than those where jet collimation takes place.

Optical spectral indices for an ADAF can vary considerably as a function of mass accretion rate (Narayan, Mahadevan & Quataert 1998). In contrast, the radio spectral index between $\sim 1 - 100$ GHz is always inverted with $\alpha \sim -0.4$ (Yi & Boughn 1998) compared to $\alpha \gtrsim 0$ typically for jet models. Table 5 lists the radio spectral index between the 1.49 GHz / 1.67 GHz and 5 GHz core fluxes. Core flux variability would have a significant effect on the derived spectral index due to the small frequency range: a factor of two change in the flux density ratio would result in a change by 0.6 in the derived spectral index. For the spectral index between 1.49 GHz and 5 GHz, for which the observations have similar resolution, 7 out of 10 sources have spectra with $\alpha > -0.4$. For the spectral index between 1.67 GHz and 5 GHz only 2 out of 10 have $\alpha > -0.4$. However, in the latter case α is a lower limit as the 5 GHz flux is measured at lower resolution than the 1.67 GHz VLBA measurements.

We conclude that at the *arcsecond* scale the radio cores are most likely dominated by the typical flat spectrum of a jet component instead of a second non-relativistic component. However, it is unclear at this point whether jet synchrotron or a second component, such as ADAF synchrotron and/or inverse Compton emission, dominates the $0.1''$ scale optical and $0.01''$ scale radio

core emission in all UGC FR I galaxies. Addressing this issue will require knowledge of the core SEDs from radio to X-ray frequencies, constraints on jet viewing angles and accretion flow and jet modeling.

5. $H\alpha$ + $[NII]$ emission excitation mechanism

Both the compactness of the core $H\alpha$ + $[NII]$ emission and its strong correlation with the radio and optical core emission from the AGN indicate that the emission gas is excited by an AGN-related process. The existence of young nuclear star clusters, which could also produce the compact $H\alpha$ + $[NII]$ emission, appears unlikely (cf. Section 4.1). Excitation by old stars from the host galaxy appears implausible as well, because the core $H\alpha$ + $[NII]$ luminosity does not correlate with either host magnitude or central stellar surface brightness (as measured just outside the optical core; cf. Table 3). Two viable AGN-related excitation mechanisms are photo- and shock-ionization. On the one hand the gas is very close to the AGN which is generally believed to produce a significant amount of photo-ionizing photons. On the other hand jets are present, which might shock the central gas. For extended gas at kiloparsec scales in nearby radio-loud galaxies (both FR I and FR IIs) both excitation mechanisms often provide good fits to the observed optical emission-line ratios (e.g., Baum, Heckman & van Breugel 1992; Simpson & Ward 1996). This degeneracy can be lifted by observing UV emission-lines, for which the relative intensities are significantly larger in the case of shock-ionization compared to photo-ionization (Allen, Dopita & Tsvetanov 1998). This approach shows for M87 that the gas as close as 50 pc from the nucleus is almost certainly shock-excited (Dopita et al. 1997). As a reference, the core $H\alpha$ + $[NII]$ flux in M87 contributes about 20% to the total flux inside an aperture with a 50 pc radius and this radius is typically about the size of the FWHM ($\sim 0.12''$) of our $H\alpha$ + $[NII]$ cores. M87 is a special case in the sense that it sits at the center of a cooling flow which might cause enhancement of shock excitation. Photons ionizing the gas can be produced by the accretion disk and jet. However, any photo-ionizing flux from the jet is highly beamed even for the relatively low Lorentz factors inferred in Section 4.3. The typical opening angle due to boosting, $1/\gamma$ (e.g., Rybicki & Lightman 1979) is 30° and 10° for $\gamma = 2$ and $\gamma = 5$ respectively. Photo-ionization by the accretion disk appears more likely.

Thus AGN processes certainly excite the central gas in the UGC FR I galaxies but it cannot be determined at this point whether shock- or photo-ionization is the dominant mechanism. We have recently obtained HST/STIS optical spectra which can shed more light on this issue (Noel-Storr et al. 2000).

6. Connections between FR Is and low-luminosity AGNs

6.1. AGN-type LINERS

How similar are the central engines of UGC FR I nuclei and AGN-type LINER nuclei which have radio cores but no large-scale radio jets? The radio and optical core emission properties of the

three AGN-type LINERS discussed in Section 4.1 roughly follow the core emission correlations found for the UGC FR I sample galaxies. For this reason we construct a larger sample of nearby early-type galaxies with LINER type nuclei and radio core emission. Ho et al. (1995,1997) identified LINER nuclei among a sample of 486 nearby galaxies in the RSA catalogue (RSA; Sandage & Tammann 1981). Many of these LINER nuclei were surveyed for radio core emission by Wrobel & Heeschen (1991). Ho (1999a) concluded that the radio core emission in these LINER nuclei with radio core emission is non-thermal and most likely produced by an AGN. In support of this interpretation, Falcke et al. (2000) inferred brightness temperatures $T_B \gtrsim 10^8\text{K}$ from higher resolution radio observations for a few AGN-type LINERS. Further support for an AGN interpretation comes from the fact that the five UGC FR I nuclei in the Ho et al. sample (NGC 315, NGC 4261, NGC 4374, NGC 4486 and NGC 7626) are also classified as LINER nuclei. The UGC FR I host galaxies are classified as E and S0 galaxies (see paper I). The morphology classification in paper I and in Ho et al. (1995) is not always consistent: NGC 315 is classified as an E in paper I but as a S0 in Ho et al. and vice versa for NGC 4374. We therefore selected all non-dwarf galaxies in the Ho et al. sample (and not in the UGC FR I sample) which (i) have morphologies which include ‘E’ or ‘S0’ in their description, (ii) have an optical spectral classification which includes ‘LINER’ in their description and (iii) were surveyed for radio emission by Wrobel & Heeschen (1991). The emission-line flux for this ‘LINER sample’ of 23 galaxies was measured through an aperture centered on the nucleus which was typically $2'' \times 4''$ (Ho et al. 1997). The VLA measurements at 5 GHz by Wrobel & Heeschen (1991) have a FWHM of $5''$. For 16 galaxies HST/ WFPC2 *V*- and/or *I*-band imaging is available. We determined the NOS fluxes and upper limits in these galaxies applying the same procedure as used for the UGC FR I sample (see Section 2.3). Only two LINER sample galaxies have a NOS detection. Radio and optical core and central $\text{H}\alpha + [\text{NII}]$ fluxes for the LINER sample are listed in Table 6. The errors in these core fluxes are similar to those of the UGC FR I sample.

Figure 8, which is similar to Figure 2, shows the core emissions for both the UGC FR I and LINER sample galaxies. For the UGC FR I sample Figure 8 plots the $\text{H}\alpha + [\text{NII}]$ emissions inside a radius of $1''$ (paper I) instead of the unresolved core $\text{H}\alpha + [\text{NII}]$ emissions of Figure 2 to provide a better match to the apertures used for the LINER sample. All but five of the LINER sample galaxies have radio core luminosities below those of the UGC FR I sample. These five galaxies are discussed in more detail below. The $\text{H}\alpha + [\text{NII}]$ luminosities of the two samples overlap, but the average $\text{H}\alpha + [\text{NII}]$ luminosity is lower for the LINER sample. It is not clear if the NOS luminosities for the two samples overlap as 14 of the 16 measurements are upper limits.

The core radio flux density and central $\text{H}\alpha + [\text{NII}]$ flux in the LINER sample nuclei do not show the tight correlation observed in the UGC FR I nuclei. At similar core radio flux densities, the $\text{H}\alpha + [\text{NII}]$ fluxes of the LINER sample are typically more than 1 order of magnitude larger than those of the UGC FR I sample. An offset remains when one takes the radio core emission for the UGC FR I sample at different resolutions (i.e., the 1.4 GHz or 5 GHz VLA observations). The cores of the UGC FR I sample are expected to have flat radio SEDs as function of ν so frequency differences are not expected to alter the observed offset significantly. In the luminosity-luminosity plane the LINER sample seems less offset, but this could be due to the fact that both quantities depend on distance. The offset is smaller for the elliptical LINER galaxies than later-type LINER galaxies. In fact, the elliptical LINER galaxies are consistent with following the luminosity correlation of the

UGC FR I sample. This was also noted by Ho (1999a) who argued that a correlation is present even after taking into account the common dependence on distance and host magnitude. The $H\alpha+[NII]$ emission for the two samples is integrated over similar apertures, while the core emission for the UGC FR I sample is observed at much smaller resolution than the core emission for the LINER sample. The offset therefore could suggest that the UGC FR I and elliptical LINER galaxies have an additional source of radio emission compared to the later-type LINER sample galaxies. The jets, clearly present in UGC FR Is at kpc scales, are a plausible source for the extra radio core emission in at least the UGC FR I galaxies. Alternatively, the enhanced emission-line luminosity in later-type galaxies might reflect a larger amount of interstellar matter present in these galaxies. Core radio and emission-line observations for LINER galaxies at similar spatial resolutions as the UGC FR I sample observations are needed to confirm the observed trends.

Figure 8 plots I -band optical core emission for all UGC FR I and most of the LINER sample. For a few LINER sample galaxies V - or R -band measurements are used. The V - and I -band optical core measurements generally differ by less than 50% (cf. Section 2.3) for the UGC FR I sample. This difference is well within the scatter of the correlations. The V - and I -band measurements differ by less than 50% as well for NGC 4278, which is the only LINER sample galaxy with a NOS detection in both bands. It is not possible to draw any firm conclusions from the two correlations which involve the optical core flux measurements, because most optical core flux measurements are upper limits. The LINER sample is only consistent with following the two core emission correlations as observed for the UGC FR I sample.

There are five LINER sample galaxies that have radio core luminosities comparable to those observed in the UGC FR I sample: NGC 4278, NGC 4589, NGC 5322, NGC 5353, and NGC 5354. Both NGC 5353 and NGC 5354 have a compact radio source unresolved at sub-arcsecond resolution (Wrobel 1991; Filho, Barthel & Ho 2000). NGC 4589 is unresolved at $5''$ resolution (Wrobel & Heeschen 1991). Both NGC 4278 and NGC 5322 have a jet-like extended radio component (Wrobel & Heeschen 1984; Feretti et al. 1984). In this respect it is also interesting that there is evidence for a jet like structure in NGC 6500 (Falcke et al. 2000) and NGC 3031 (Falcke & Biermann 1999), which are two of the LINERS discussed in Section 4.1. HST/WFPC2 imaging is available for NGC 5322, NGC 4589 and NGC4278. An apparently edge-on dust disk obscures the galaxy nucleus in NGC 5322 and inhibits a NOS flux measurement. The NOS detection and upper limit in NGC 4278 and NGC 4589 respectively are consistent with being on the radio - optical core and $H\alpha+[NII]$ - optical core correlation (both in flux and luminosity) observed for the UGC FR I sample. It will be worthwhile to obtain narrow-band and spectroscopic observations for the AGN-type LINERS at higher spatial resolutions as performed for the UGC FR I sample (cf. Section 5). Such observations should clarify to which extent the optical continuum flux is contaminated by line-emission. For the optical continuum emission in UGC FR I nuclei the contribution from line emission is small (cf. Section 2.3) but this is not necessarily the case for the weaker cores in AGN-type LINERS (Cappellari et al. 1999).

The conclusion is that AGN-type LINERS as a class do not seem to follow the same core emission correlations as the UGC FR I sample in general. The core emissions in LINER ellipticals however might lie on the same correlations, but higher resolution radio and emission-line observations are needed to confirm this. If true, this and the offset in the distribution of radio core

and central $H\alpha+[NII]$ fluxes between the UGC FR I and elliptical LINERS on the one hand, and later-type AGN-type LINERS on the other hand and the detection of small-scale jets in some of the LINER galaxies then suggest: (i) the central engines in FR I galaxies and AGN-type LINERS with elliptical hosts are similar but the latter class are a down-scaled version of the former, and (ii) the core emission, both at VLA and VLBA scales, is dominated by inner jet emission.

6.2. Kinematically Decoupled Cores

One of the two NOS detections in the LINER sample, NGC 4278, has a kinematically distinct stellar core (KDC). This galaxy is part of a HST/WFPC2 study of 18 elliptical galaxies with a KDC by Carollo et al. (1997a,b). They found an unresolved optical core in four galaxies with $V - I$ colors similar to the UGC FR I optical cores. Analysis of the nuclear emission in NGC 4278 and NGC 4552 suggests that both host a low-luminosity AGN (Ho, Filippenko & Sargent 1997; Cappellari et al. 1999). Thus it is reasonable to assume that the optical core emission in the other two KDC galaxies is produced by a low-luminosity AGN as well. In fact, the KDC galaxies also have radio core and central $H\alpha+[NII]$ emission (cf. Table 6). The squares in Figure 8 show that also the radio and optical core and central $H\alpha+[NII]$ emissions of KDCs roughly follow the correlations observed for the UGC FR I cores. The $\sim 20\%$ optical core detection rate in KDCs at luminosities comparable to those observed in FR I nuclei suggest that perhaps the peculiar central dynamics of KDCs play a role in triggering nuclear activity. Interestingly, one UGC FR I galaxy, NGC 7626, hosts a KDC as well.

7. Summary & Conclusions

In this paper we have analyzed the relation between $0.01''$ scale radio and $0.1''$ scale optical continuum and $H\alpha+[NII]$ core emission of a complete sample of 21 nearby FR I galaxies. The main conclusions are:

1. We confirm the linear correlation between optical and radio core emission in nearby FR I nuclei. We find that both core emissions also correlate with the core $H\alpha+[NII]$ emission. The mutual correlations are unlikely to be caused by obscuration from the ubiquitous central dust.
2. Nuclear stellar clusters are highly unlikely to be the source of the optical core emission for two reasons. First, previous spectral studies have directly excluded a nuclear stellar cluster for two typical members of the UGC FR I sample. Second, the UGC FR I radio, optical and $H\alpha+[NII]$ core luminosities resemble the nuclei of AGN-type LINERS more closely than stellar-type LINERS. An AGN origin for the optical cores in all UGC FR I galaxies is strongly suggested by the tight correlation with radio core emission, which is certainly produced by the AGN.
3. A jet origin for both the radio and optical core emission is favored because (i) optical and radio core emission are tightly correlated, (ii) spectral indices from radio to optical are similar

to those for extended optical jets, (iii) there is a suggestive trend with independent estimates from jet orientation, and (iv) the correlation residuals from both core emission with $H\alpha+[NII]$ emission are correlated. However, a significant contribution from a second component, such as accretion disk/flow/wind, to the radio and optical emission at the $0.1''$ scale for the optical and the $0.01''$ scale for the radio emission might be present.

4. The correlation of the optical and radio core emission with the isotropic $H\alpha+[NII]$ emission constrains the core bulk Lorentz factor $\gamma \lesssim 2$ if the inner jets consist of discrete blobs ($p = 3$). For a continuous jet, bulk Lorentz factors $\gamma \sim 2 - 5$ are inferred. This result critically depends on the assumed range in viewing angle, which is assumed to be $[30^\circ, 90^\circ]$. The bulk Lorentz factors required by the BL Lac - FR I unification scheme are generally larger, i.e. $\gamma > 5$. If the core emission is dominated by a jet component, this discrepancy could be reconciled by a two-layer jet with a fast moving spine surrounded by a slower outer layer.
5. The central gas is excited by AGN-related processes. Both shock- and photo-ionization appear plausible excitation mechanisms at this time.
6. Radio, optical and $H\alpha+[NII]$ core luminosities of elliptical LINER-type AGNs with and without kiloparsec-scale radio jets appear to have similar relations. The results suggest (i) the engines in the two types producing the cores might be similar and (ii) the core radio emission is dominated by inner jet emission.

Conclusions 1 to 5 prompt us to make the following speculation: if the radio and optical core emission are indeed inner jet synchrotron emission, then their strong correlation with $H\alpha+[NII]$ core emission implies either a direct link between jet luminosity and gas excitation power, possibly via jet - gas interactions or a close relation between AGN photo-ionizing power and jet radiative (and possibly kinetic) power.

Conclusion 6 and the close resemblance of quiescent and radio-loud active galaxies from scales just outside the AGN to the entire galaxy and even environment lead to two further speculations. First, either all bright early-type galaxies can host an AGN, or the capability of a bright early-type galaxy to become an AGN is set by conditions within the central few parsecs, currently unresolved at most wavelengths. Second, the capability of a LINER-type AGN to become radio-loud is set by conditions at similar scales. Two main ingredients for an active nucleus are present at these scales: accreting matter and a supermassive black hole. Likely factors determining the formation of large-scale radio jets are then the black hole spin and/or the inner accretion disk properties. A rigorous comparison between the nuclei of active and quiescent nearby galaxies at the tens of parsec resolution could advance our understanding on these issues.

Support for this work was provided by NASA through grant number #GO-06673.01-95A from the Space Telescope Science Institute, which is operated by AURA, Inc., under NASA contract NAS5-26555. It is a pleasure to thank Michele Cappellari for careful reading of the manuscript and useful suggestions and the referee for helpful suggestions that improved the manuscript. We thank Aaron Barth for pointing out a significant typo in an earlier version of the paper.

A. Isophotal analysis of UGC 7115 and 3C 449

We present observations and the isophotal analysis for UGC 7115 and 3C 449 (UGC 12064). Together with the 19 galaxies presented in paper I these galaxies form a well-defined complete sample of FR I galaxies. For UGC 7115 we present new HST/WFPC2 *V*- and *I*-band imaging, while for 3C 449 we are using archival WFPC2 *R*-band and narrow-band imaging presented in Martel et al. (1999) and Martel et al. (2000) (see Figure 9). The data reduction for these two galaxies and the rest of the sample was done in similar fashion and is discussed in detail in paper I. Some general properties for the two galaxies are listed in Table 7 and the observation logs are presented in Table 8.

A.1. UGC 7115

UGC 7115 is a relatively isolated galaxy. The nearest galaxy at similar distance as catalogued by NED⁴ is at 9.5'. Figure 9 shows the WFPC2 *V*-band image of UGC 7115. We detect an almost round dust disk (axis ratio ~ 0.95) with a diameter of 1.3'' (570 pc). The rim of the disk appears darker than its inner region. UGC 7115 has a central blue nuclear optical source (see Section 2.3). We compare our isophotal results (see Figure 10) with isophotal results for $r = 2'' - 20''$ from cousins *R*-band imaging of UGC 7115 by Fasano & Bonoli (1989) taken under bad seeing. The predicted *R* magnitude from the *V* and *I* band imaging is ~ 1 magnitude brighter than observed by Fasano & Bonoli. Moreover, they derive an isophotal PA $\sim 90^\circ$ for $r = 5'' - 10''$ which increases to 110° inwards. The cause of the ~ 1 magnitude difference in photometric calibration and the $\sim 90^\circ$ offset in PA is unknown. The latter difference might be due to the bad seeing. Lambas, Groth & Peebles (1988) report a PA= 170° consistent with our results. The ellipticity derived by Fasano & Bonoli agrees to within ~ 0.02 . UGC 7115 has a one-sided jet structure (Xu et al. 2000).

A.2. 3C 449 (UGC 12064)

3C 449 has a companion at $\sim 37''$ and is part of Zwicky cluster 2231.2 +3732. The HST/WFPC2 *R*-band imaging for 3C 449 was presented by Martel et al. (1999) and is shown in Figure 9. The galaxy has a central dust disk 3.5'' (1.2kpc) in diameter with a mottled morphology and was detected by Capetti et al. (1994). The disk is aligned with the stellar major axis. Our estimate of the disk inclination is $57 \pm 3^\circ$, assuming the disk is intrinsically circular. This inclination is a bit lower than the $\sim 65^\circ$ reported by Martel et al. (1999). The $H\alpha + [NII]$ emission is concentrated on the nucleus and there is a spot at 1.3'' North from nucleus on the inside of the dust ring. We compare our isophotal analysis (see Figure 10) with De Juan, Colina & Pérez-Fouron (1994), who used ground-based observations. The ellipticity profile agrees well outside the dust disk radius and ϵ increases towards 0.3 between $r = 10'' - 30''$. The PA agrees as well and continues to increase

⁴The NASA/IPAC Extragalactic Database (NED) is operated by the Jet Propulsion Laboratory, California Institute of Technology, under contract with the National Aeronautics and Space Administration.

to 240° at $r = 30''$. 3C 449 has a well-known twin-jet radio structure (Feretti et al. 1999, and references therein).

B. Beaming parameters

We want to estimate how Doppler boosting affects the observed relation between two fluxes f_1 and f_2 for which the rest-frame fluxes f'_1 and f'_2 are related by a power law defined as

$$\log f'_2 = a_{\text{int}} \log f'_1 + b_{\text{int}}. \quad (\text{B1})$$

The primed quantities are measured in the rest frame of the emitter. The flux f_1 is not affected by beaming ($f_1 = f'_1$) but the monochromatic flux f_2 is. The flux $f_\nu(\nu)$ and $f'_{\nu'}(\nu')$ for an emitting particle are related by (e.g., Urry & Padovani, 1995):

$$f_\nu(\nu) = \delta^p f'_{\nu'}(\nu'), \quad (\text{B2})$$

where ν and ν' are related as $\nu = \delta\nu'$ and the kinematic Doppler factor δ is defined as

$$\delta = [\gamma(1 - \beta \cos \theta)]^{-1}, \quad (\text{B3})$$

with $\gamma = \sqrt{1/(1 - \beta^2)}$ the Lorentz factor and β the velocity of the emitting material in units of the speed of light, and θ the angle of the velocity vector with the line of sight. The factor p depends on the structure of the jet and the spectral index of the emitting material (cf. Urry & Padovani 1995). For example, for an isotropically emitting smooth continuous jet $p = 2 + \alpha$, while for a moving discrete source with isotropic emission $p = 3 + \alpha$, where α is the rest-frame spectral index defined as $f'_{\nu'} \sim (\nu')^{-\alpha}$. We consider the case where the flux f_2 is emitted by a symmetric two-sided Doppler boosted jet and hence the relation between f_2 and f'_2 is

$$\log f_2 = \log f'_2 + \log \frac{\delta^p(\theta) + \delta^p(\pi + \theta)}{2} \equiv \log f'_2 + \mathcal{B}, \quad (\text{B4})$$

where \log indicates the logarithm of base 10. We will refer to \mathcal{B} as the logarithmic Doppler boosting factor.

A linear least-squares regression fit to a sample of logarithmic flux pairs f_1, f_2 will yield a slope a_{obs} and intercept b_{obs} (in the absence of measurement errors):

$$\begin{aligned} a_{\text{obs}} &= a_{\text{int}} + \frac{\overline{f_1 \mathcal{B}} - \overline{f_1} \cdot \overline{\mathcal{B}}}{\overline{f_1^2} - \overline{f_1}^2} \\ b_{\text{obs}} &= b_{\text{int}} + \overline{\mathcal{B}}, \end{aligned} \quad (\text{B5})$$

where the overlining denotes the mean of the quantity. We assume that \mathcal{B} does not depend on either f'_1 or f'_2 . In that case we obtain $a_{\text{obs}} = a_{\text{int}}$. Thus the observed slope of the linear regression fit for a sample of (f_1, f_2) pairs will equal the slope of the intrinsic relation between f'_1 and f'_2 and the observed residuals will equal $\mathcal{B} - \overline{\mathcal{B}}$. If we assume that the sample has spherically randomly distributed jet viewing angles in the range $\theta = [\theta_0, \theta_1]$ and a known identical bulk Lorentz factor γ

and jet structure parameter p we can evaluate the mean and standard deviation of the logarithmic Doppler boosting factor by

$$\begin{aligned}\overline{\mathcal{B}} &= \int_{\theta_0}^{\theta_1} \mathcal{B} \sin \theta d\theta / \int_{\theta_0}^{\theta_1} \sin \theta d\theta \\ \sigma^2(\mathcal{B}) &= \overline{\mathcal{B}^2} - \overline{\mathcal{B}}^2,\end{aligned}\tag{B6}$$

The integral for $\overline{\mathcal{B}}$ can be expressed in terms of elementary functions for integer p . The result for $p = 1, 2, 3$:

$$\begin{aligned}y &\equiv \beta \cos \theta, \\ C &\equiv \frac{\log e}{y_1 - y_0}, \\ I_0 &\equiv [-p \ln(\gamma) y]_{y_0}^{y_1}, \\ I_1 &\equiv -[(1 + y) \ln(1 + y) - (1 + y)]_{y_0}^{y_1}, \\ I_2 &\equiv [(1 - y) \ln(1 - y) - (1 - y)]_{y_0}^{y_1}, \\ I_3 &\equiv [y \ln(y^2 + 1) - 2y + 2 \arctan(y)]_{y_0}^{y_1}, \\ I_4 &\equiv \frac{1}{\sqrt{3}} [\sqrt{3} y \ln(3y^2 + 1) - 2\sqrt{3} y + 2 \arctan(\sqrt{3} y)]_{y_0}^{y_1}, \\ \overline{\mathcal{B}} &= C(I_0 + I_1 + I_2), & \text{for } p = 1, \\ \overline{\mathcal{B}} &= C(I_0 + 2[I_1 + I_2] + I_3), & \text{for } p = 2, \\ \overline{\mathcal{B}} &= C(I_0 + 3[I_1 + I_2] + I_4), & \text{for } p = 3.\end{aligned}\tag{B7}$$

The integral for $\overline{\mathcal{B}^2}$ must be evaluated numerically. The intercept shift $\overline{\mathcal{B}}$ is not directly observed, because b_{int} is unknown. However, the residual, $\mathcal{B} - \overline{\mathcal{B}}$, and the variance of the regression fit $\overline{\mathcal{B}^2}$ are both observable. Thus one can determine which combinations of γ and p are consistent with the observed residuals of the regression fit and their variance.

REFERENCES

- Allen G.A., Dopita M.A., Tsvetanov Z.I., 1998, ApJ, 493, 571
 Barth A.J., Ho L.C., Filippenko A.V., & Sargent W.L.W., 1998, ApJ, 496, 133
 Baum S.A., Heckman T.M., 1989, ApJ, 336, 681
 Baum S.A., Heckman T.M., van Breugel W., 1992, ApJ, 389, 208
 Baum S.A., Zirbel E.L., O’Dea C.P., 1995, ApJ, 451, 88
 Baum S.A., et al. , 1997, ApJ, 483, 178
 Becker R.H., White R.L., Helfand D.J., 1995, ApJ, 450, 559
 Biretta J.A., Stern C.P., Harris D.E., 1991, AJ, 101, 1632
 Biretta J.A., Zhou F., Owen F.N., 1995, ApJ, 447, 582
 Biretta J.A., Perlman E., Sparks W.B., Macchetto F., 1999 in The radio galaxy Messier 87, ed. H.-J. Röser, K. Meisenheimer, (Berlin: Springer), 210
 Bower G.A., et al. , 2000, ApJ, 534, 189
 Bridle A.H., Perley R.A., 1984, ARA&A, 22, 319
 Browne I.W.A., 1983, MNRAS, 204, 23

- Butcher H.R., van Breugel W., Miley G.K., 1980, *ApJ*, 235, 749
- Cappellari M., et al. , 1999, *ApJ*, 519, 117
- Capetti A., Macchetto F.D., Sparks W.B., Miley G.K., 1994, *A&A*, 289, 61
- Capetti A., de Ruiter H.R., Fanti R., Morganti R., Parma P., Ulrich M.-H., 2000 *A&A*, 362 871
- Carollo C.M., Franx M., Illingworth G.D., Forbes D.A., 1997a, *ApJ*, 481, 710
- Carollo C.M., Danziger I.J., Rich R.M., Chen, X., 1997b, *ApJ*, 491, 545
- Carter D., Jenkins C.R., 1992, *MNRAS*, 257, 7p
- Chiaberge M., Capetti A., Celotti A., 1999, *A&A*, 349, 77
- Chiaberge M., Celotti A., Capetti A., Ghisellini G., 2000, *A&A*, 358, 104
- Condon J.J., Broderick J.J., 1988, *AJ*, 96, 30
- Condon J.J., Cotton W.D., Greisen E.W., Yin Q.F., Perley R.A., Taylor G.B., Broderick J.J., 1998 *AJ*, 115, 1693
- Colina L., de Juan L., 1995, *ApJ*, 448, 548
- Crane P., et al. , 1993, *ApJ*, 402, L37
- De Juan L., Colina L., Pérez-Fouron I., 1994, *ApJS*, 91, 507
- de Koff S., et al. , 2000, *ApJS*, 129, 33
- Di Matteo T., Quataert E., Allen S.W., Narayan R., Fabian A.C., 2000, *MNRAS*, 311, 507
- Dopita M.A., Koratkar, A.P., Allen M.G., Tsvetanov Z.I., Ford H.C., Bicknell G.V., Sutherland R.S., 1997, *ApJ*, 490, 202
- Dressler A., Richstone, D.O., 1990, *ApJ*, 348, 120
- Faber S.M., et al. , 1989, *ApJS*, 69, 763
- Falcke H., Biermann P.L., 1999, *A&A*, 342, 49
- Falcke H., Nagar N.M., Wilson A.S., Ulvestad J.S., 2000, *ApJ*, 542, 197
- Fanaroff B.L., Riley F.M., 1974, *MNRAS*, 167, 31
- Fasano G., Bonoli C., 1989, *A&AS*, 79, 291
- Isobe T., Feigelson E.D., Nelson P.L., 1986, *ApJ*, 306, 490
- Feretti L., Giovannini G., Hummel E., Kotanyi C.G., 1984, *A&A*, 137, 362
- Feretti L., Perley R., Giovannini G., Andernach H., 1999, *A&A*, 341, 29
- Ferrarese L., Ford H.C., Jaffe W., 1996, *ApJ*, 470, 444
- Filho M.E., Barthel P.D., Ho L.C., 2000, *ApJS*, 129, 93F
- Ford H.C., et al. , 1994, *ApJ*, 435, L27
- Giovannini G., Cotton W.D., Feretti L., Lara L., Venturi T., 2001, *ApJ*, 551, in press
- Gonzalez-Serrano J.I., Carballo R., 1993, *AJ*, 105, 1710

- Goudfrooij P., Hansen L., Jørgensen H.E., Nørgaard-Nielsen H.U., 1993, *A&AS*, 105, 341
- Hardcastle M.J., Alexander P., Pooley G.G., Riley J.M., 1996, *MNRAS*, 278, 273
- Hardcastle M.J., Worrall D.M., 2000, *MNRAS*, 314, 359
- Heckman T.M., O’Dea C.P., Baum S.A., Laurikainen E., 1994, *ApJ*, 428, 65
- Ho L.C., Filippenko A.V., Sargent W.L., 1995, *ApJS*, 98, 477
- Ho L.C., Filippenko A.V., Sargent W. L. W., Peng C.Y., 1997, *ApJS*, 112, 391
- Ho L.C., 1999a, *ApJ*, 510, 631
- Ho L.C., 1999b, *ApJ*, 516, 672
- Hummel E., van der Hulst J.M., Dickey J.M., 1984, *A&A*, 134, 207
- Jarvis B.J., Melnick J., 1991, *A&ALetters*, 244, 1
- Junor W., Biretta J.A., Livio M., 1999, *Nature*, 401, 891
- Knapp, G.R., Guhathakurta P., Kim D.-W., Jura M.A., 1989 *ApJS*, 70, 329
- Knapp G.R., Bies W.E., van Gorkom J.H., 1990, *AJ*, 99, 476
- Kommisarov 1990, *SvA Letters* 16, 284
- Kormendy J., 1992, *ApJ*, 388, L9
- Krolik J., in “Active Galactic Nuclei”, 1999, Chapter 9.2 (Princeton University Press)
- Lambas D.G., Groth E.J., Peebles P.J.E., 1988, *AJ*, 95, 975
- Laing R.A., Parma P., de Ruiter H.R., Fanti R., 1999, *MNRAS*, 306, 513
- Lara L., Feretti L., Giovannini G., Baum S., Cotton W.D., O’Dea C.P., Venturi T., 1999, *ApJ*, 513, L197
- Ledlow M.J., Owen F.N., 1995, *AJ*, 110, 1959
- Ledlow M.J., Owen F.N., Yun M.S., Hill J.M., 2001, *ApJ*, 552, 120
- Macchetto F., et al. , 1996, *A&AS*, 120, 463
- Maoz D., Filippenko A.V., Ho L.C., Rix H.-W., Bahcall J.N., Schneider D.P., Macchetto F.D., 1995, *ApJ*, 440, 91
- Maoz D., Koratkar A., Shields J.C., Ho L.C., Filippenko, A.V., Sternberg A., 1998, *AJ*, 116, 55
- Martel A.R., et al. , 1998, *ApJ*, 496, 203
- Martel A.R., et al. , 1999, *ApJS*, 122, 81
- Martel A.R., Turner N.J., Sparks W.B., Baum S.A., 2000, *ApJS*, 130, 267
- Morganti R., Ulrich M.-H., Tadhunter C.N., 1992, *MNRAS*, 254, 546
- Narayan R., Mahadevan R., Quataert E., in *The Theory of Black Hole Accretion Discs*, eds. M.A. Abramowicz, G Bjornsson & J.E. Pringle (CUP), in press, astro-ph/9803141.
- Nicholson K.L., Reichert G.A., Mason K.O., Puchnarewicz E.M., Ho L.C., Shields J.C., Filippenko A.V., 1998, *MNRAS*, 300, 893

- Nilson P., 1973, *Uppsala General Catalogue of Galaxies* (Uppsala Astronomical Observatory), Uppsala
- Noel-Storr J., et al. 2001, in “The central kpc of starbursts and AGN: the La Palma connection”, eds. J.H. Knapen, J.E., Beckman, I. Shlosman and T.J. Mahoney, ASP conf. series, in press [astro-ph/0106397]
- Owen F.N., Hardee P.E., Cornwell T.J., 1989, ApJ, 340, 698
- Philips M.M., Jenkins C.R., Dopita M.A., Sadler E.M., Binette L., 1986, AJ, 91, 1062
- Press, W. H., Teukolsky, S. A., Vetterling, W. T., & Flannery, B. P. 1992, *Numerical Recipes* (Cambridge: Cambridge University Press)
- Quataert E., Di Matteo T., Narayan R., 1999, ApJ, 525, L89
- Reynolds C.S., Di Matteo T., Fabian A.C., Hwang U., Canizares C.R., 1996, MNRAS, 283, L111
- Rybicki G.B., Lightman A.P., 1979, *Radiative Processes in Astrophysics*, (Wiley, New York)
- Sadler E.M., Slee O.B., Reynolds J.E., Roy A.L., 1995, MNRAS, 276, 1373
- Sandage & Tamman 1981, *A Revised Shapley-Ames Catalog of Bright Galaxies*, Carnegie Institute of Washington Pub. No. 635 (RSA)
- Simpson C., & Ward M., 1996, MNRAS, 282, 797
- Sparks W.B., et al. , 1995 ,ApJ, 450, 55L
- Sparks W.B., Baum S.A., Biretta J., Macchetto F.D., Martel A.R., 2000, ApJ, 542, 667
- Shukla H., Stoner R.E., 1996 ApJS, 106, 41
- Tran H.D., Tsvetanov Z., Ford H.C., Davies J., Jaffe W., van den Bosch F.C., Rest A., 2001, AJ, in press
- Tsvetanov Z.I., et al. , 1999, in *The radio galaxy Messier 87*, eds. H.-J. Röser, K. Meisenheimer, 307
- Turner J.L., Ho P.T.P., 1994, ApJ, 421, 122
- Urry C.M., Padovani P., 1995, PASP, 107, 803
- van der Marel R.P., 1994, MNRAS, 270, 271
- van der Marel R.P., van den Bosch, F.C., 1998, AJ, 116, 2220
- Verdoes Kleijn G.A., Baum S.A., de Zeeuw, P.T., O’Dea C.P., 1999, AJ, 118, 2592 (paper I)
- Verdoes Kleijn, G.A., van der Marel, R.P., Carollo C.M., de Zeeuw P.T., 2000, AJ, 120, 1221
- Voit M. (ed.), et al. , 1997, *HST Data Handbook, Volume I, Update Version 3.1 March 1998*, STScI, Baltimore
- White R.L., Becker R.H., Helfand D.J., Gregg M.D., 1997, ApJ, 475, 479
- Wrobel, J.M., Heeschen, D.S., 1984, ApJ, 287, 41
- Wrobel J.M., 1991, AJ, 101, 127
- Wrobel, J.M., Heeschen, D.S., 1991, AJ, 101, 148

- Wrobel J.M., Machalski J., Condon J.J., 2001, in preparation
- Xu C., Baum S.A., O’Dea C.P., Wrobel J.M., Condon J.J., 2000, *AJ*, 120, 2950
- Yi I., Boughn S.P., 1998, *ApJ*, 499, 198
- Yi I., Boughn S.P., 1999, *ApJ*, 515, 576
- Zirbel E.L., 1993, Ph.D. thesis, Yale University
- Zirbel E.L., 1996, *ApJ*, 473, 144
- Zirbel E.L., Baum S.A., 1995, *ApJ*, 448, 521
- Zirbel E.L., Baum S.A., 1998, *ApJS*, 114, 177

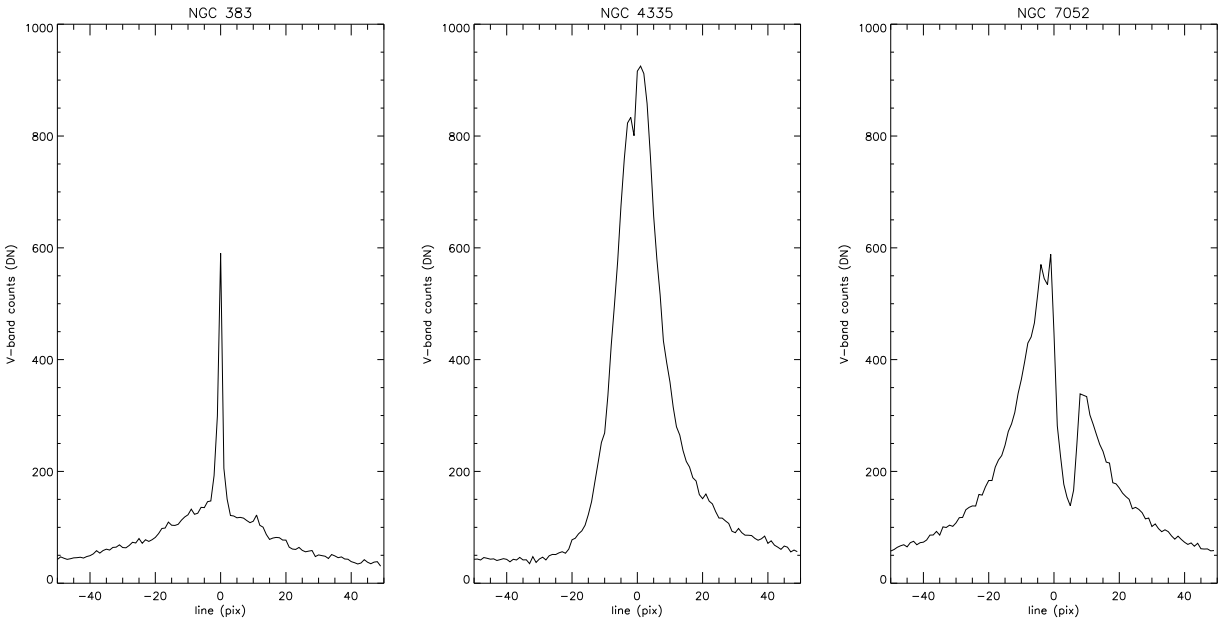


Fig. 1.— Three examples of the central V -band flux profile (DN counts) along the WFPC2/PC CCD line which crosses the galaxy nucleus in the WFPC2 image. NGC 383 (left) has an unresolved nuclear optical source (NOS) which clearly stands out from the shallow-sloped stellar background (the WFPC2/PC PSF has a FWHM of ~ 2.2 pixels). NGC 4335 (middle) has a bright and steeply rising stellar flux profile which makes the detection of the expected NOS flux very difficult. The central flux profile in NGC 7052 (right) is severely affected by dust obscuration which inhibits a reliable determination of the NOS flux. See Section 2.3 for a complete discussion of the NOS measurements.

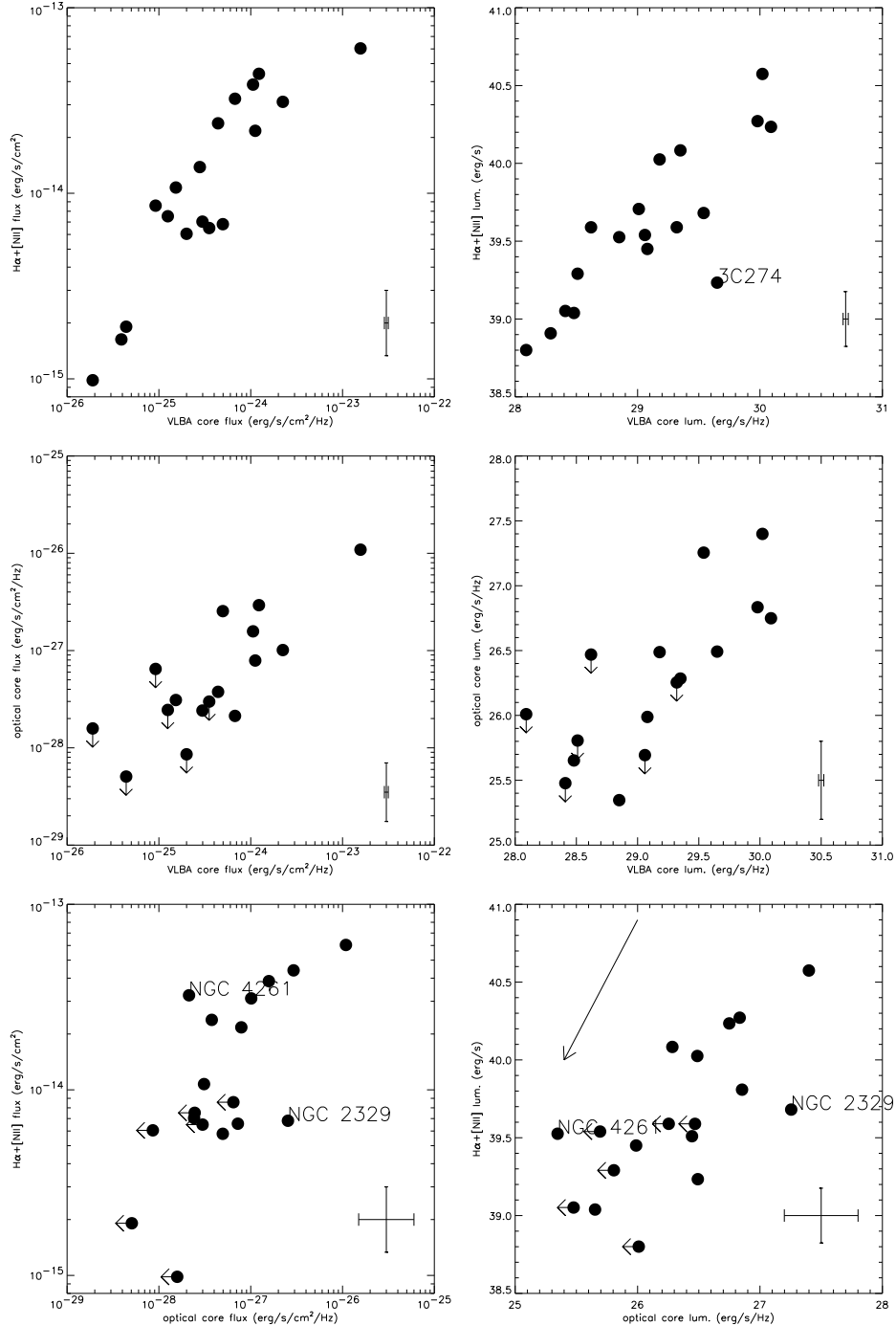


Fig. 2.— The VLBA radio core, WFPC2 optical core, and core $\text{Ha}+\text{[NII]}$ emission in the UGC FR I nuclei plotted versus each other. The left column contains flux-flux plots, the right column contains luminosity-luminosity plots. Arrows indicate upper limits. The correlation between each pair of quantities is significant at more than the 99% level according to a generalized Kendall’s tau test (see Tables 2 and 3). The error bars in the lower right corner of each plot indicate the typical error for each quantity. The large arrow in the lower right plot indicates the displacement of a datapoint if it were observed through a dust screen with a V-band opacity $A_V = 3$

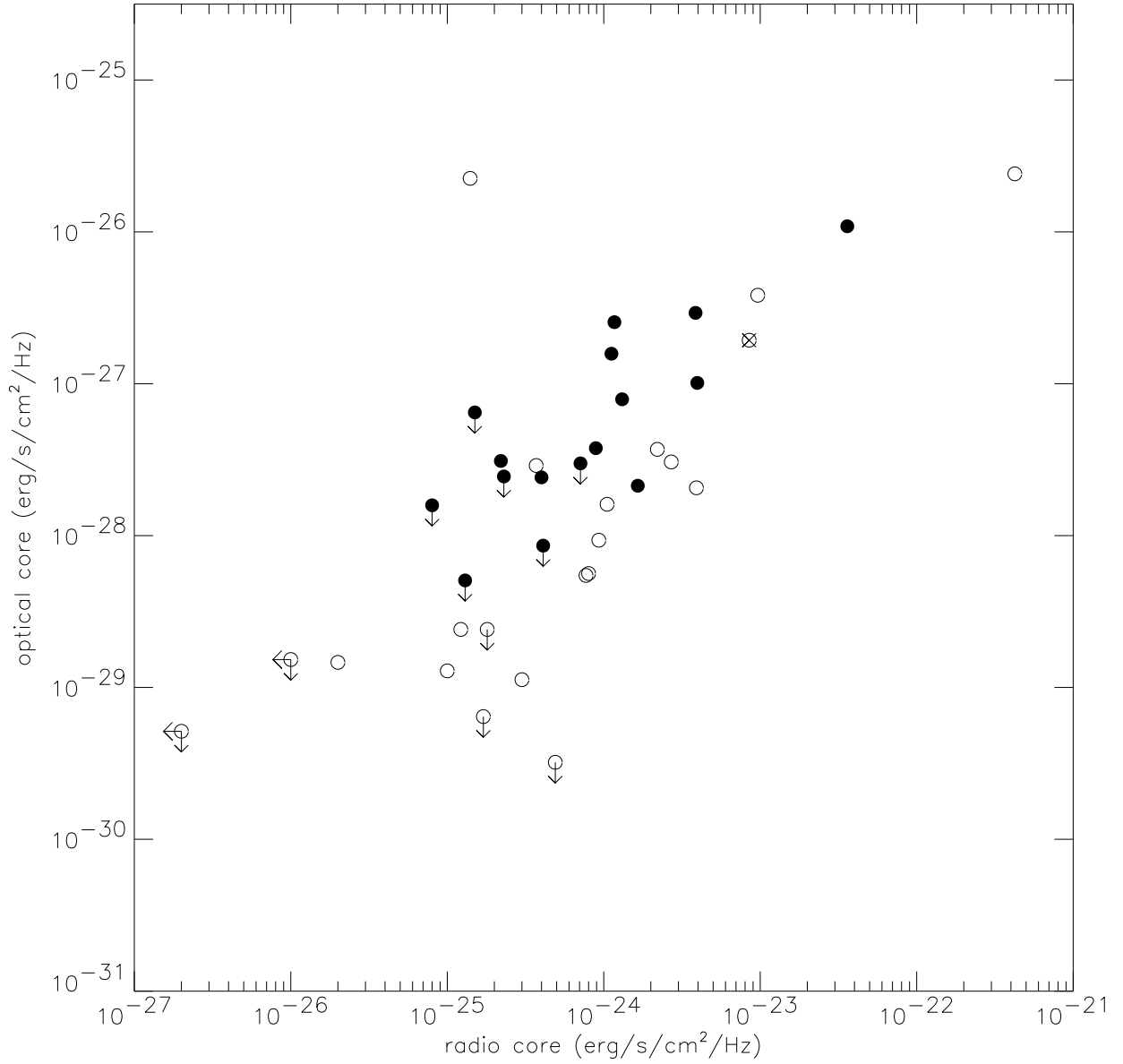


Fig. 3.— Optical WFPC2 *I*-band core flux as a function of the radio core flux for the 3CR FR I sample (open circles; Chiaberge, Capetti & Celotti 1999) and for our UGC FR I sample (filled circles; we plot our core emission measurements for the sources overlapping with the 3CR sample). The crossed circle is NGC 6251 from Hardcastle & Worrall (2000). Arrows indicate upper limits. For the UGC sample the radio core flux at 1.49 GHz is plotted, while for the other galaxies the 5 GHz core flux is plotted (see Section 3.2 for discussion). The outlier is the peculiar galaxy 3C 386 (see Section 3.2). The combined sample shows a highly significant linear correlation between radio and optical core flux.

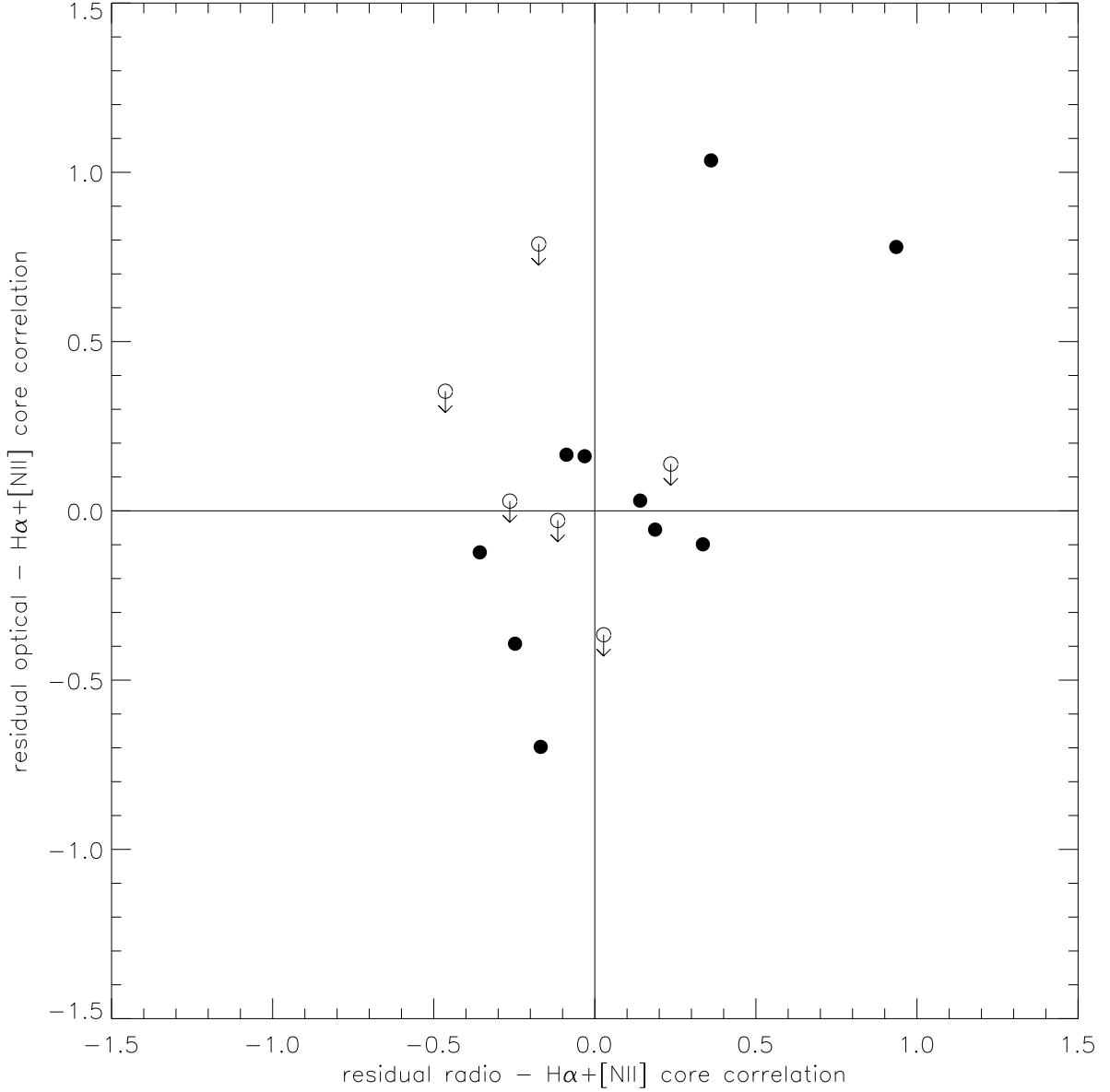


Fig. 4.— Both radio and optical core luminosity are well correlated with the central $H\alpha+[NII]$ luminosity in log-log space (Figure 2). This plot shows the residuals of the linear regression fit to these two correlations. The linear regression fits consider the $H\alpha+[NII]$ luminosity as the independent variable. The arrows indicate the upper limits to the optical core emission. The two residuals are again well correlated, especially when taking the typical errors in the fluxes into account (cf. Figure 2). This supports the idea that the radio and optical core emission have a common origin, as discussed in Sections 3 and 4.3.

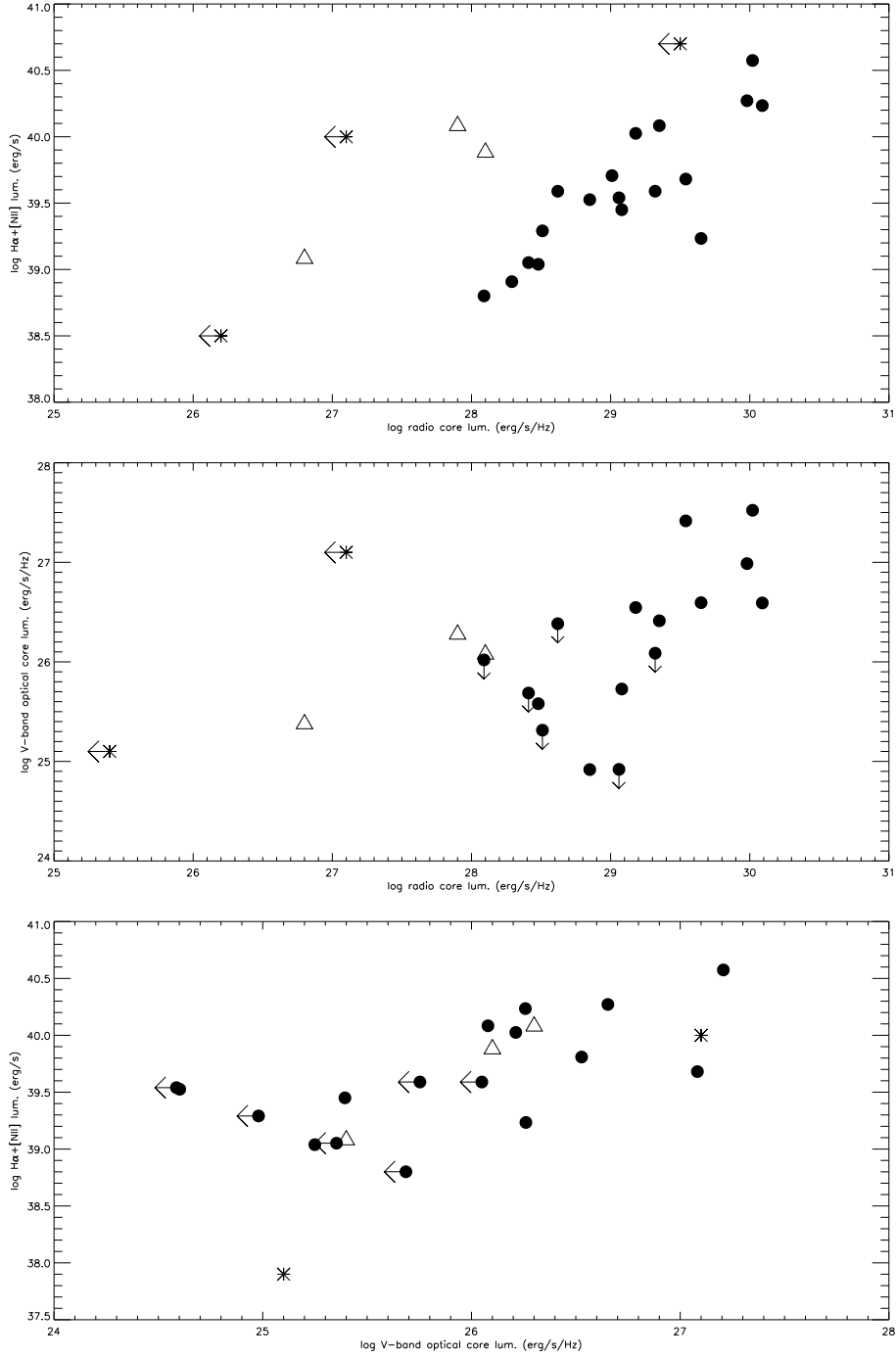


Fig. 5.— The correlations between the core luminosities for the UGC FR I galaxies (dots) but now with the data for the UV-bright LINER sample indicated as well (Maoz et al. 1998; cf. Table 4). Stellar-type LINER galaxies are denoted by stars and AGN-type LINERS are denoted by triangles. Arrows denote upperlimits. The AGN-type LINER and UGC FR I core emissions roughly overlap, while the stellar-type LINERS deviate, mainly in their radio luminosities. This suggests an AGN origin for all three fluxes in UGC FR I nuclei (see Section 4.1).

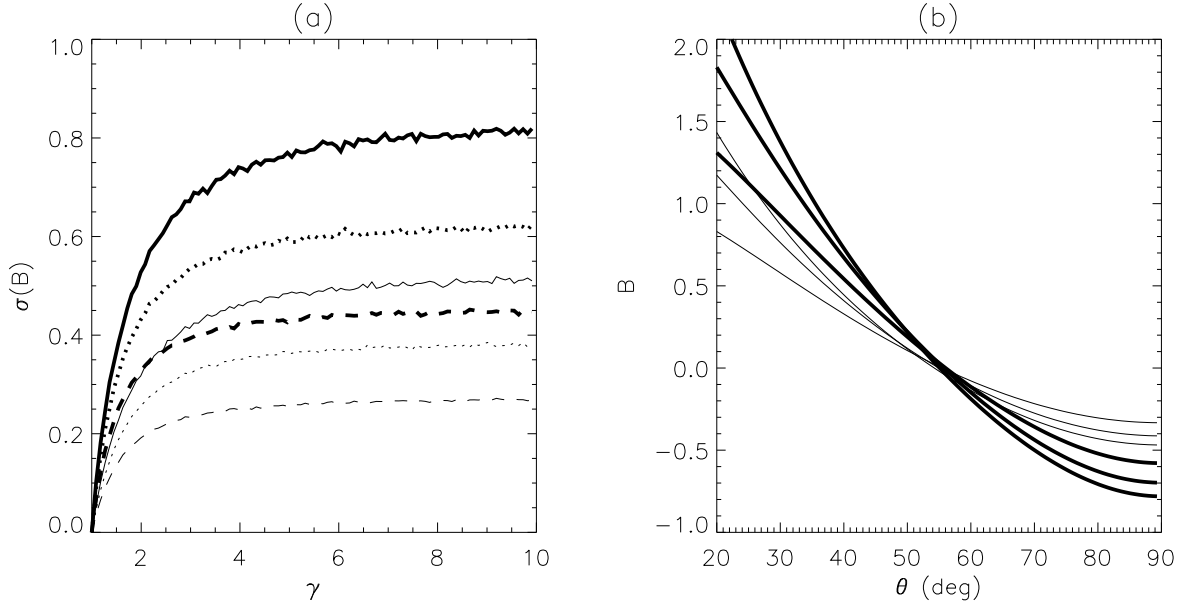


Fig. 6.— Doppler boosting of jet radio emission causes scatter around the linear regression fit of the observed logarithmic radio flux as a function of $\text{H}\alpha + [\text{NII}]$ flux (see Section 3.1 and Appendix B). **(a)**: the predicted standard deviation of this scatter $\sigma^2(\mathcal{B})$ is plotted as a function of the jet bulk Lorentz factor γ for a continuous jet ($p = 2$, thin curves) and a jet consisting of discrete blobs ($p = 3$, thick curves). For both models the rest-frame flux is emitted isotropically and has a flat spectrum (i.e., $\alpha = 0$). Jet viewing angles are spherically randomly distributed in the range $[20^\circ, 90^\circ]$ (solid curves), $[30^\circ, 90^\circ]$ (dotted curves) and $[40^\circ, 90^\circ]$ (dashed curves).

The observed standard deviation is ~ 0.3 . Any inferred bulk Lorentz factor is in fact an upper limit because there are probably other sources of scatter such as measurement errors and flux variability. **(b)**: the predicted residual, $\mathcal{B} - \overline{\mathcal{B}}$, from the correlation is plotted as a function of jet viewing angle θ for a continuous jet (thin curves) and a jet consisting of discrete blobs (thick curves). The jet parameters are identical to those under (a). The three curves per jet type are for $\gamma = 2$, $\gamma = 3$ and $\gamma = 5$ (i.e., increasing maximum and minimum residuals). The observed range of residuals is $\sim [-0.5, 1.0]$.

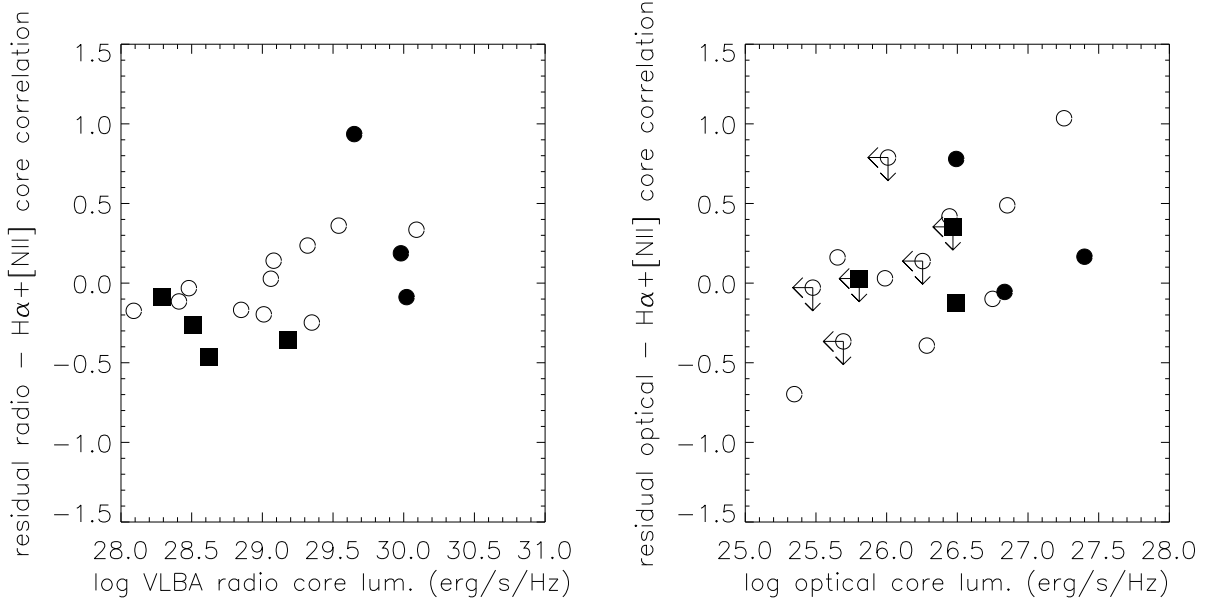


Fig. 7.— Left: the residuals of the linear regression fits to the radio core luminosity as a function of $H\alpha$ + [NII] core luminosity (in log-log space) plotted as a function of radio core luminosity. Consistent with a Doppler boosting origin for the residuals all galaxies with jets expected to be oriented close to the plane of the sky (filled squares) have negative residuals, while galaxies with jets expected to be oriented close to the line of sight (filled circles) have close to positive or positive residuals. These expectations are based on jet properties (see Section 4.3). Additional support for the beaming scenario is the trend that more luminous cores have more positive residuals. Right: similar plot as the left panel but now for the optical core emission. The plot is consistent with the conclusions drawn for the radio cores. The increase in scatter in this plot is expected from the larger measurement error in the optical core flux compared to the radio core flux. Both trends are mainly driven by the few points at the high and low end of the distributions and hence larger samples are required to confirm these results.

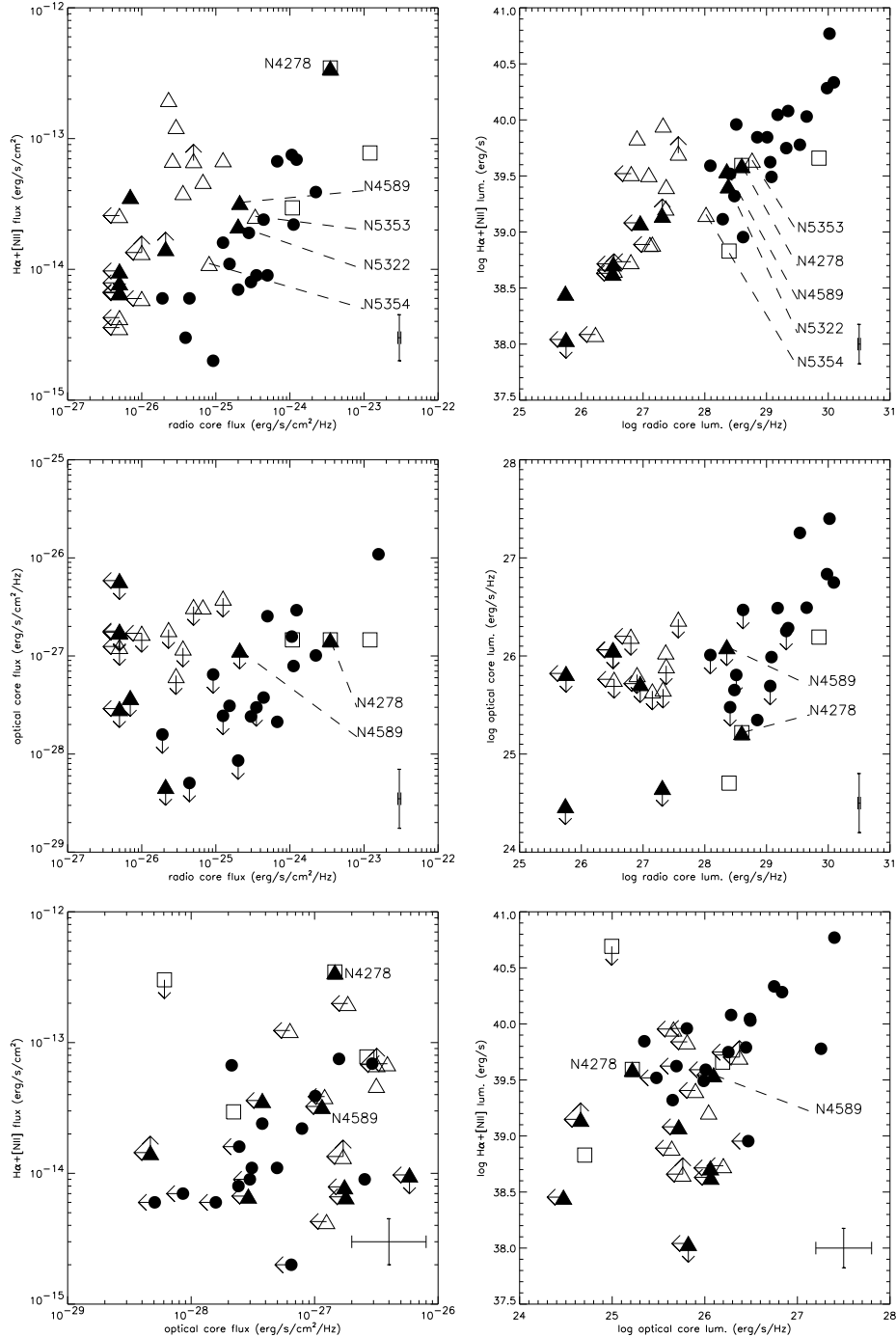


Fig. 8.— This figure is similar to Figure 2 and plots the radio core, optical core and central $\text{Ha}+\text{[NII]}$ emission of the UGC FR I nuclei (solid dots), LINER sample nuclei (triangles) and ellipticals with kinematically decoupled cores (KDCs, squares) discussed in Section 6. The solid triangles are elliptical galaxies and the open triangles are E/S0 and S0 galaxies (see Table 6). Arrows indicate upper limits and the error bars in the lower right corner of each panel indicate the typical errors. The plots suggest that the elliptical LINER and KDC nuclei follow the core emission correlations observed for the UGC FR I sample. See Section 6 for further discussion.

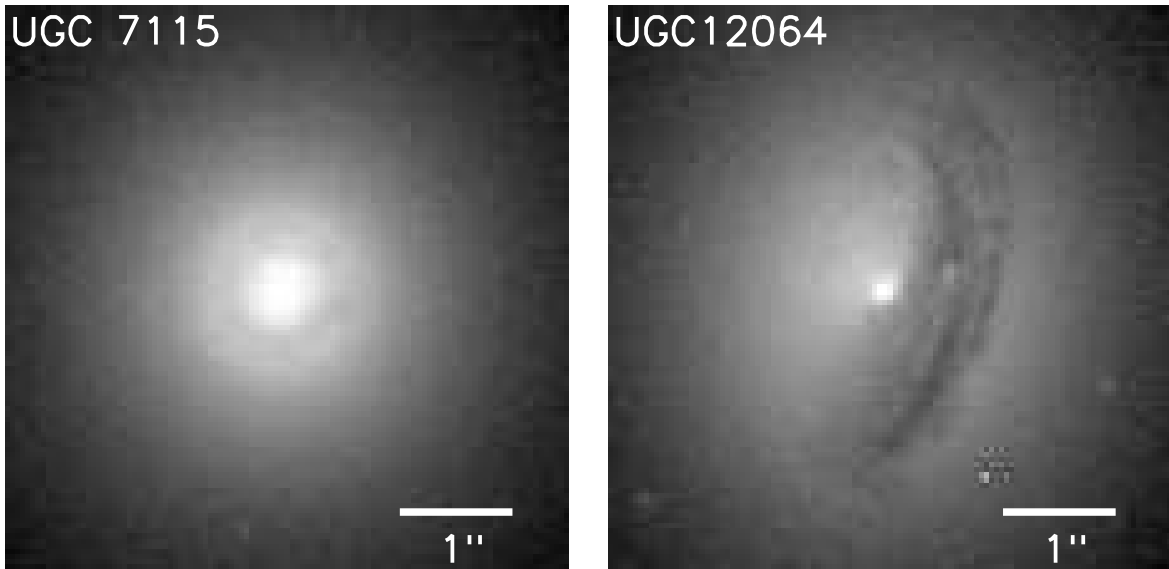


Fig. 9.— *V*-band image of UGC 7115 and *R*-band image of 3C 449 (UGC 12064). The images have logarithmic stretch. North is up and East is to the left.

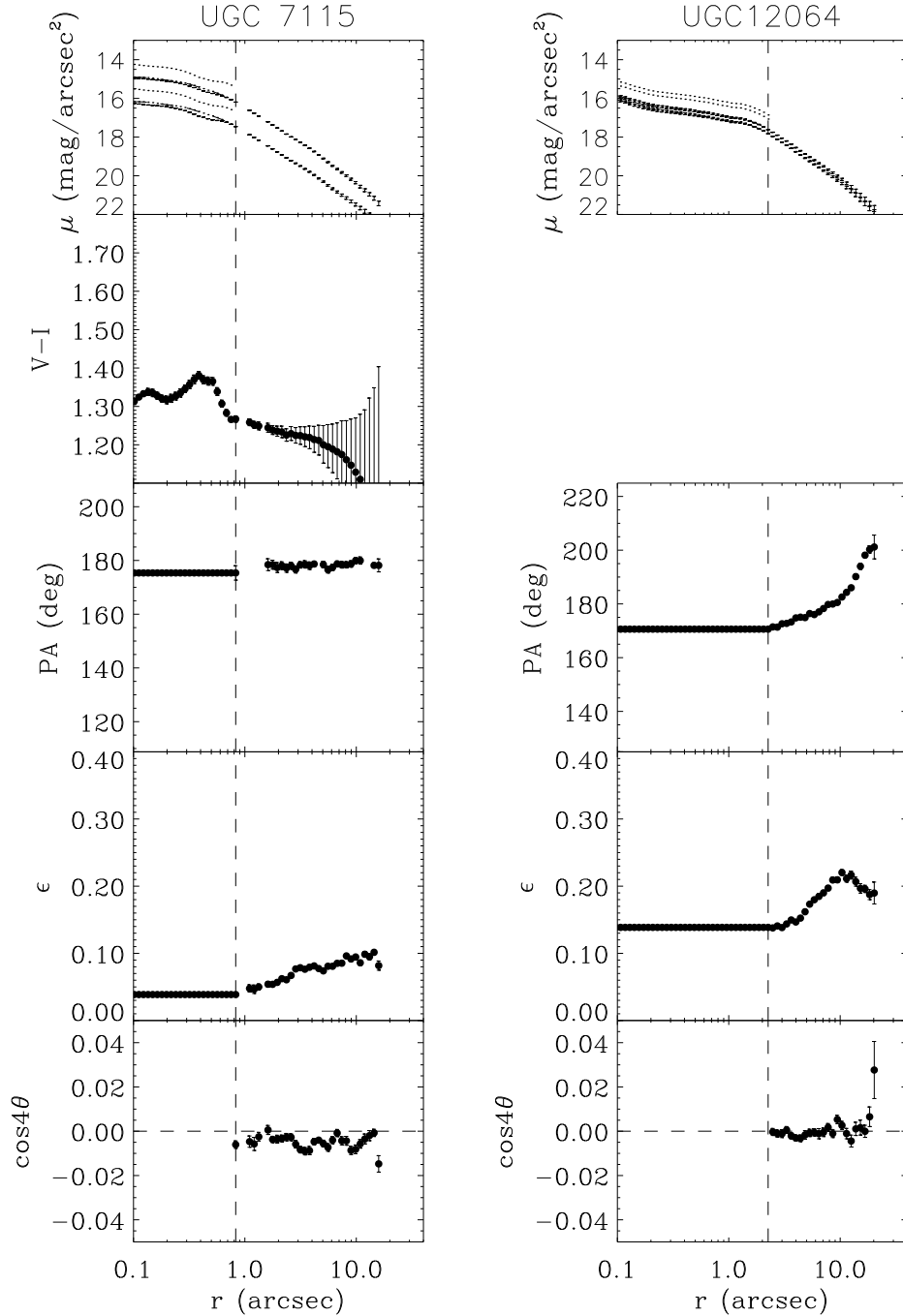


Fig. 10.— Isophotal parameters in the I -band (UGC 7115) and R -band (3C 449) as a function of radius along the major axis. From top to bottom: surface brightness, $V-I$ color, position angle, ellipticity and fourth order Fourier coefficient. The galaxy name is shown above each column. The top plot for UGC 7115 also shows the V -band luminosity profile (i.e. higher μ). The dashed and dotted lines display luminosity profiles corrected for dust obscuration (see paper I). Error bars include the formal error given by the isophotal fitting routine and the error in the estimated sky counts. The vertical dashed line indicates the maximum radius out to which the isophotes are affected by dust obscuration and PA and ϵ are kept fixed.

Table 1. HST/WFPC2 core fluxes

Name 1 (1)	Name 2 (2)	Filter V (3)	NOS flux V (4)	Filter I (5)	NOS flux I (6)	$H\alpha+[NII]$ flux (7)
NGC193		F555W	6.2e-18	F814W	1.1e-17	7.0e-15
NGC315		F555W	3.3e-17	F814W	4.7e-17	3.1e-14
NGC383		F555W	2.4e-17	F814W	1.8e-17	2.4e-14
NGC541		F555W	<7.5e-18	F814W	<7.4e-18	9.8e-16
NGC741		F555W	<3.8e-18	F814W	<2.4e-18	1.9e-15
UGC1841	3C66B	F555W	5.2e-17	F814W	3.7e-17	2.2e-14
NGC2329		F555W	1.7e-16	F814W	1.2e-16	6.8e-15
NGC2892		F555W	1.6e-17	F814W	1.4e-17	1.1e-14
NGC3801		F555W	†	F814W	†	<3.3e-16
NGC3862	3C264	F547W	1.9e-16	F791W	1.4e-16	4.4e-14
UGC7115		F555W	3.4e-17	F814W	3.4e-17	6.6e-15
NGC4261	3C270	F547W	3.8e-18	F791W	1.0e-17	3.2e-14
NGC4335		F555W	<2.5e-17	F814W	<3.0e-17	8.6e-15
NGC4374	3C272.1	F547W	6.2e-17	F814W	7.3e-17	3.9e-14
NGC4486	3C274	F555W	6.4e-16	F814W	3.2e-16	6.0e-14
NGC5127		F555W	†	F814W	†	1.6e-15
NGC5141		F555W	<9.5e-18	F814W	<1.4e-17	6.5e-15
NGC5490		F555W	<6.7e-19	F814W	<4.0e-18	6.1e-15
NGC7052		F547W	†	F814W	†	1.4e-14
UGC12064	3C449	‡	-	F702W	3.1e-17	5.8e-15
NGC7626		F555W	<3.7e-18	F814W	<1.1e-17	7.5e-15

Note. — The optical and $H\alpha+[NII]$ core fluxes from WFPC2 observations. Col.(3)-(6): V - and I -band filter NOS flux in $\text{erg s}^{-1} \text{cm}^{-2} \text{\AA}^{-1}$. Upper limits are given for sources in which no optical core was detected (i.e., $\text{FWHM} > 0.08''$; see Section 2.3). Notes: †: nucleus hidden from view by dust. ‡: no WFPC2 V -band observation available. Col.(7): $H\alpha+[NII]$ core flux in $\text{erg s}^{-1} \text{cm}^{-2}$.

Table 2. Core flux correlations

Flux 1 (1)	Flux 2 (2)	Cox (3)	Kendall (4)	Schmitt(slope,intercept) (5)	LR(slope,intercept) (6)
VLBA core	H α + [NII]	0.0001	0.0001	0.58(0.09) 0.45(2.19)	0.66(0.08) 2.08
Host magn.	H α + [NII]	0.0212	0.0783		
Radio tot	H α + [NII]	0.0060	0.1730		
5 GHz core	H α + [NII]	0.0232	0.0240		
VLA core	H α + [NII]	0.0002	0.0004	0.64(0.13) 1.40(3.27)	0.63(0.10) 1.38
VLBA core	NOS <i>I</i>	0.0002	0.0006		
VLBA core	NOS <i>V</i>	0.0003	0.0009		
NOS <i>I</i>	H α + [NII]	-	0.0035		
NOS <i>V</i>	H α + [NII]	-	0.0046		
VLBA ext.	H α + [NII]	0.0038	0.0044	0.61(0.14) -1.27(3.38)	0.59(0.13) 0.87
VLA ext.	H α + [NII]	0.0435	0.1107		
VLBA core	VLBA ext.	< 0.0001	< 0.0001		

Note. — Statistical significance of various flux-flux correlations and the linear regression fits to the logarithm of the fluxes. Col.(1)-(2): the pair of fluxes under consideration. Flux 1 and 2 are the independent and dependent variable, respectively. Fluxes are in $\text{erg s}^{-1} \text{cm}^{-2}$ or $\text{erg s}^{-1} \text{cm}^{-2} \text{Hz}^{-1}$; host magnitude is the apparent photographic magnitude (paper I). The abbreviation ext. refers to extended flux. Col.(3)-(4): probability no correlation is present between the two quantities using Cox’s proportional hazard model. Col.(5)-(6): the slope and intercept of a linear regression fit using Schmitt’s method and with Kaplan-Meier residuals (Isobe, Feigelson & Nelson 1986). The errors on the parameters are given between parentheses.

Table 3. Core luminosity correlations

Lum. 1 (1)	Lum. 2 (2)	Cox (3)	Kendall (4)	Schmitt(slope,intercept) (5)	LR(slope,intercept) (6)
VLBA core	H α + [NII]	< 0.0001	0.0001	0.68(0.11) 19.71(3.24)	0.69(0.11) 19.61
Host magn.	H α + [NII]	0.3138	0.3465	-0.27(0.19) 34.28(3.88)	-0.27(0.19) 34.29
Radio tot.	H α + [NII]	0.1049	0.4171	0.26(0.21) 31.72(6.52)	0.26(0.19) 31.59
5 GHz core	H α + [NII]	0.0523	0.0734	0.47(0.26) 25.81(7.58)	0.48(0.23) 25.46
VLA core	H α + [NII]	0.0001	0.0002	0.65(0.12) 20.39(3.49)	0.65(0.12) 20.58
VLBA core	NOS <i>I</i>	0.0001	0.0003	-	1.18(0.25) -8.45
VLBA core	NOS <i>V</i>	0.0004	0.0007	-	1.47(0.35) -17.27
NOS <i>I</i>	H α + [NII]	-	0.0057	-	0.55(0.17) 25.31 [†]
NOS <i>V</i>	H α + [NII]	-	0.0062	-	-
VLBA ext.	H α + [NII]	0.0006	0.0013	0.60(0.09) 22.38(2.62)	0.60(0.11) 22.63
VLA ext.	H α + [NII]	0.0881	0.0635	-	-
VLBA core	VLBA ext.	< 0.0001	0.0001		
H α + [NII]	IRAS 12 μ m	0.9483	0.3272	-	-
H α + [NII]	IRAS 25 μ m	0.1967	0.6872	-	-
H α + [NII]	IRAS 60 μ m	0.2768	0.0351	-	-
H α + [NII]	IRAS 100 μ m	0.6445	0.9195	-	-
NOS <i>I</i>	IRAS 12 μ m	-	0.5400	-	-
NOS <i>I</i>	IRAS 25 μ m	-	0.4550	-	-
NOS <i>I</i>	IRAS 60 μ m	-	0.1347	-	-
NOS <i>I</i>	IRAS 100 μ m	-	0.8119	-	-
inclination	H α + [NII]	0.1496	0.3918	-	-
inclination	NOS <i>I</i>	0.2056	0.1691	-	-
inclination	NOS <i>V</i>	0.1601	0.1105	-	-
inclination	NOS <i>V</i> – <i>I</i>	0.9224	0.7538	-	-
inclination	res. radio core - H α + [NII]	0.5136	0.6767		
inclination	res. radio core - NOS <i>I</i>	0.3003	0.2990		
μ_I	H α + [NII]	0.5209	0.5848		

Note. — Statistical significance of various luminosity-luminosity correlations and linear regression fits to the logarithm of the luminosities. The columns are similar to those in Table 2. All luminosities are in erg s^{-1} or $\text{erg s}^{-1} \text{Hz}^{-1}$; host magnitude is the absolute photographic magnitude (paper I). The abbreviation ext. refers to extended emission, inclination refers to dust-disk inclination, res. refers to residuals from the correlations and μ_I is the central stellar surface brightness. Notes: [†]: a least squares linear regression method which takes into account the errors in the measurements of both quantities is used in this case, because the errors in both measurements are similar (Press et al. 1992).

Table 4. Central emission in UV-bright LINERs

Target	Type	Filter	D ₇₅ (Mpc)	NOS (erg s ⁻¹ Hz ⁻¹)	H α + $[\text{NII}]$ (erg s ⁻¹)	Radio (erg s ⁻¹ Hz ⁻¹)
(1)	(2)	(3)	(4)	(5)	(6)	(7)
NGC 0404	S0	F547M	2.4	25.0	37.8	< 25.4 ^a
NGC 3031	Sab	F547M	3.6	25.4	39.1	26.8 ^b
NGC 4569	Sab	F547M	12.3	27.0	40.0	< 27.1 ^a
		F791W		-		
NGC 4579	Sb	F547M	18.5	26.2	40.1	27.9 ^c
		F791W		26.6		
NGC 4594	Sa	F547M	12.0	26.0	39.9	28.1 ^d
		F814W		26.5		
NGC 5055	Sb	F606W	8.3	-	38.5	< 26.2 ^a
NGC 6500	Sab	F547M	40.0	-	40.0	< 29.5 ^e

Note. — Central radio, optical continuum and H α + $[\text{NII}]$ luminosities for the LINER galaxy sample studied by Maoz et al. (1998). Col. (2): Hubble type. Col. (3): HST/WFPC2 filter for which the optical emission was determined. Col. (4): galaxy distances from Maoz et al. (1998). Col. (5): the unresolved nuclear optical luminosity. For the NGC 4569 F791W image and NGC 6500 F547M image no unresolved source could reliably be detected. The core was saturated in the image of NGC 5055. Col. (6): central H α + $[\text{NII}]$ luminosity, typically measured within a central aperture of a few arcsec² (Ho, Filippenko & Sargent 1997). The fluxes for NGC 3031, NGC 4569 and NGC 5055 were obtained under non-photometric conditions and might be underestimated. Col. (7): (upper limits to) the core radio luminosity at 1.4 GHz. References for the radio luminosities ^a:upper limits from peak flux measurements obtained from the FIRST radio sky survey which has resolution of FWHM $\sim 5''$ (White et al. 1997); ^b: Turner & Ho (1994); ^c: Sadler et al. (1995); ^d:Hummel, van der Hulst, & Dickey (1984); ^e:upper limits from peak flux measurements obtained from the NVSS radio sky survey which has resolution of FWHM $\sim 45''$ (Condon et al. 1998). The detections have resolutions of FWHM $\leq 1''$.

Table 5. Radio Core Spectral Indices

target	α_1	α_2	target	α_1	α_2
(1)	(2)	(3)	(1)	(2)	(3)
NGC 193			NGC 4261	-1.43	-0.53
NGC 315	-0.79	-0.23	NGC 4335		
NGC 383	1.39	1.85	NGC 4374	-0.13	-0.07
NGC 541			NGC 4486	-0.73	0.04
NGC 741			NGC 5127	-1.60	-0.95
3C66B	-0.42	-0.25	NGC 5141	-1.30	-0.58
NGC 2329			NGC 5490		
NGC 2892			NGC 7052	-0.53	-0.26
NGC 3801			3C449		
NGC 3862	-0.46	0.55	NGC 7626		
UGC 7115					

Note. — Radio spectral indices (defined by $S_\nu \sim \nu^{-\alpha}$). Col.(2): radio spectral index of VLBA 1670 MHz core (FWHM $\sim 0.01''$) and 5 GHz core (FWHM $\sim 1.4''$ except NGC 4261: FWHM $\sim 15''$). The typical error due to the VLBA flux uncertainty is 0.04. The errors for the 5 GHz fluxes are unknown. Col.(3): radio spectral index VLA 1490 MHz core (FWHM $1.5'' - 3.75''$) and 5 GHz core with a typical error of 0.04 due to the VLA flux uncertainty. Core variability might have a significant effect on the derived spectral index because the fluxes were not observed at the same epoch (see Section 4.4).

Table 6. Central emission in LINER and KDC galaxies

Target	Type	D ₇₅ (Mpc)	Filter	NOS ($\text{erg s}^{-1} \text{cm}^{-2} \text{Hz}^{-1}$)	H α + $[\text{NII}]$ ($\text{erg s}^{-1} \text{cm}^{-2}$)	Radio ($\text{erg s}^{-1} \text{cm}^{-2} \text{Hz}^{-1}$)
(1)	(2)	(3)	(4)	(5)	(6)	(7)
NGC 474	RS0/a	32.5	F814W	<1.25E-27	4.28E-15	<5.00E-27
NGC 3193	E2	23.2	F702W	<1.79E-27	6.61E-15	<5.00E-27
NGC 3226	E2/S0.1(2)	23.4	F547M	<1.21E-27	3.87E-14	3.60E-26
NGC 3379	E0	8.1	F814W	<3.77E-28	3.61E-14	7.00E-27
NGC 3414	S0.(1-2)/a	24.9	F814W	<3.19E-27	>6.78E-14	5.00E-26
NGC 3607	S0.3(3)	19.9	F814W	†	6.83E-14	2.60E-26
NGC 3608	E1	23.4	F814W	<1.75E-27	7.88E-15	<5.00E-27
NGC 4036	S0.3(8)/a	24.6	F547M	<6.31E-28	1.24E-13	2.90E-26
NGC 4111	S0.1(9)	17.0	F547M	<1.86E-27	1.99E-13	2.30E-26
NGC 4143	S0.1(5)/a	17.0	F606W	3.16E-27	4.71E-14	6.70E-26
NGC 4203	S0.2(1)	9.7	F814W	<3.89E-27	6.89E-14	1.25E-25
NGC 4278	E1	9.7	F814W	1.46E-27	3.46E-13	3.51E-24
NGC 4494	E1	9.7	F814W	<5.87E-27	<9.72E-15	<5.00E-27
NGC 4550	E7/S0.1(7)	16.8	F814W	<1.70E-27	>1.35E-14	<1.00E-26
NGC 4589	E2	30.0	F814W	<1.15E-27	3.25E-14	2.10E-25
NGC 4762	S0.1	16.8	-	-	3.59E-15	<5.00E-27
NGC 5322	E4	31.6	F814W	†	2.14E-14	2.00E-25
NGC 5353	S0.1(7)/E7	37.8	-	-	2.55E-14	3.40E-25
NGC 5354	S0 (spindle)	32.8	-	-	1.11E-14	8.10E-26
NGC 5485	S0.3(2)	32.8	-	-	5.98E-15	<1.00E-26
NGC 5631	S0.3(2)/a	32.7	-	-	2.58E-14	<5.00E-27
NGC 5813	E1	28.5	F814W	<4.67E-29	>1.44E-14	2.10E-26
NGC 5982	E3	38.7	F814W	<2.90E-28	6.70E-15	<5.00E-27
NGC 4278	E1	9.7	F814W	1.46E-27	3.46E-13	3.51E-24
NGC 4552	E	13.8	F814W	2.21E-28 ¹	2.95E-14	1.08E-24 ^a
NGC 7192	E	36.8	F814W	<6.08E-29 ²	3.02E-13	-
IC 1459	E	22.1	F814W	2.65E-27 ³	7.76E-14	1.20E-23 ^b

Note. — Central radio, optical continuum and H α + $[\text{NII}]$ luminosities for the LINER galaxy sample divided by a horizontal line from similar data for the KDC sample. NGC 4278 is part of both samples. The samples are discussed in Section 6. Col. (2)-(3): Hubble type and distance from Ho et al. (1997) for the LINER sample and from Carollo et al. (1997a,b) for the KDC sample. Col. (4)-(5) Nuclear optical source filter and flux for galaxies with HST/WFPC2 observations. Note: †: central dust inhibits a reliable estimate of the NOS flux. The NOS measurements for the KDC sample are taken from Carollo et al. (1997a,b). Col. (6): central H α + $[\text{NII}]$ luminosity, typically measured within 2''x4'' for the LINER sample. Lower limits are due to non-photometric observing conditions. References for the KDC sample: ¹: Cappellari et al. (1999); ³: Macchetto et al. (1996); ⁴: Verdoes Kleijn et al. (2000). Col. (7): the VLA core radio flux at 5 GHz (FWHM

Table 7. General properties

UGC	Type	D_{75} (Mpc)	M_p (mag)	$\text{Log } L_{\text{radio}}$ (WHz^{-1})	Comment
(1)	(2)	(3)	(4)	(5)	(6)
07115	E	90.5	-20.3	23.85	
12064	E-S0	68.3	-19.9	24.29	3C 449

Note. — General properties of UGC 7115 and UGC 12064. The general properties of the other sample galaxies were presented in paper I. Col. (1): UGC number. Col. (2): Hubble type from Condon & Broderick (1988). Col. (3): distances from Faber et al. (1989) or if not available directly from recession velocity and $H_0=75 \text{ kms}^{-1}\text{Mpc}^{-1}$. Col. (4)-(5): photographic magnitude and total spectral radio luminosity at 1400 MHz from Condon & Broderick (1988). Col. (6): 3C catalog number.

Table 8. HST/WFPC2 Observational Log

Target	Filter	Exposure Time (s)
(1)	(2)	(3)
UGC 7115	F555W	1000
UGC 7115	F814W	800
3C 449	F702W	560
3C 449	LRF680	600

Note. — Observational log of UGC 7115 and 3C 449. Col. (2): HST/WFPC2 filter name Col. (3): total exposure time of each observation.